

# Distributed Auto-Learning GNN for Multi-Cell Cluster-Free NOMA Communications

Xiaoxia Xu, Yuanwei Liu, *Senior Member, IEEE*, Qimei Chen, *Member, IEEE*,  
Xidong Mu, and Zhiguo Ding, *Fellow, IEEE*

## Abstract

A multi-cell cluster-free NOMA framework is proposed, where both intra-cell and inter-cell interference are jointly mitigated via flexible cluster-free successive interference cancellation (SIC) and coordinated beamforming design, respectively. The joint design problem is formulated to maximize the system sum rate while satisfying the SIC decoding requirements and users' data rate constraints. To address this highly complex and coupling non-convex mixed integer nonlinear programming (MINLP), a novel distributed auto-learning graph neural network (AutoGNN) architecture is proposed to alleviate the overwhelming information exchange burdens among base stations (BSs). The proposed AutoGNN can train the GNN model weights whilst automatically learning the optimal GNN architecture, namely the GNN network depth and message embedding sizes, to achieve communication-efficient distributed scheduling. Based on the proposed architecture, a bi-level AutoGNN learning algorithm is further developed to efficiently approximate the hypergradient in model training. It is theoretically proved that the proposed bi-level AutoGNN learning algorithm can converge to a stationary point. Numerical results reveal that: 1) the proposed cluster-free NOMA framework outperforms the conventional cluster-based NOMA framework in the multi-cell scenario; and 2) the proposed AutoGNN architecture significantly reduces the computation and communication overheads compared to the conventional convex optimization-based methods and the conventional GNN with a fixed architecture.

## Index Terms

Cluster-free SIC, distributed optimization, graph neural network (GNN), non-orthogonal multiple access, next-generation multiple access.

X. Xu and Q. Chen are with the School of Electronic Information, Wuhan University, Wuhan, 430072, China (e-mail: {xiaoxiaxu, chenqimei}@whu.edu.cn).

Y. Liu is with the School of Electronic Engineering and Computer Science, Queen Mary University of London, London E1 4NS, U.K. (email: yuanwei.liu@qmul.ac.uk).

X. Mu is with School of Artificial Intelligence, Beijing University of Posts and Telecommunications, Beijing, 100876, China (email: muxidong@bupt.edu.cn).

Z. Ding is with the School of Electrical and Electronic Engineering, The University of Manchester, Manchester M13 9PL, U.K. (email: zhiguo.ding@manchester.ac.uk).

## I. INTRODUCTION

Next-generation wireless networks are envisioned to provide massive connectivity and high-quality transmissions for billions of bandwidth-hungry wireless devices in diversified scenarios [1], [2]. To meet these requirements, the concept of next-generation multiple access (NGMA) [3] has been proposed to adaptively and intelligently provide wireless services for multiple users/devices given the limited radio resources. Among others, the integration of multiple antenna technology with non-orthogonal multiple access (NOMA) is regarded as one of the most promising candidates for NGMA [3], which enables users to be served via the same orthogonal time/frequency resource while multiplexed in both the spatial and power domains. However, conventional multi-antenna NOMA approaches have to group users into different clusters. By doing so, intra-cluster and inter-cluster interference can be mitigated via the employment of successive interference cancellation (SIC) and the spatial beamforming. Nevertheless, the effectiveness of conventional multi-antenna NOMA approaches rely on specific scenarios, which may not always hold due to the channel randomness. To address this issue, a generalized multi-antenna NOMA transmission framework was proposed in [4] with a novel concept of cluster-free SIC. By breaking the limitation of sequentially carrying out SIC within each cluster, the proposed cluster-free NOMA is capable to achieve efficient interference suppression and high communication performance.

Despite providing an enhanced transmission flexibility, the investigations on the cluster-free NOMA communication design are in an early stage. Recall the fact that network densification is a key enabling means for enhancing the network capacity and providing ubiquitous access. On the road to NGMA, one of the most fundamental and practical problem is how to design efficient multi-cell cluster-free NOMA communications. Since multi-cell systems have to combat both intra-cell and inter-cell interference, the coordinated scheduling of base stations (BSs) is a crucial concern. However, this is usually highly computational complexity, and requires sharing the locally available channel state information (CSI) among BSs. To reduce the computational complexity and relieve overwhelming information exchange overheads, it is urgent to design efficient distributed scheduling methods.

### A. Prior Works

To handle the distributed scheduling in multi-cell networks, the methods employed in existing works can be loosely classified into two categories, namely the conventional optimization-based

and the learning-based methods.

1) *Conventional optimization-based distributed scheduling*: The authors of [7] developed two interference alignment based coordinated beamforming schemes for two-cell multiple-input multiple-output (MIMO)-NOMA networks, which successfully deal with inter-cell interference and increase the throughput of cell-edge users. The authors of [8] investigated a Karush-Kuhn-Tucker based distributed optimization method in coordinated beamforming (CoMP)-NOMA networks, where BSs locally optimize power allocation strategies. The authors of [9] investigated distributed joint user grouping, beamforming, and power control strategies to minimize the power consumption of multi-cell multiple-input single-output (MISO)-NOMA networks through zero-forcing beamforming, semiorthogonal user selection, and power consumption oriented user grouping. Additionally, to maximize the energy efficiency under imperfect SIC, the authors of [10] developed a distributed alternating direction method of multipliers (ADMM) for coordinated power allocation in a downlink heterogeneous Terahertz MIMO-NOMA network. Moreover, by considering both perfect and imperfect CSI, the authors of [11] developed a distributed ADMM-based resource allocation algorithm to maximize the energy efficiency for a massive MIMO-NOMA network.

2) *Learning-based distributed scheduling*: Deep learning (DL) has been widely considered as a promising paradigm for distributed scheduling [12]–[15]. Compared with conventional non-structural deep neural networks (DNNs) that usually require massive data samples and suffer poor generalizations and scalability [16], graph neural network (GNN) can implement distributed control by exploiting the graph topology of system environments and enabling information diffusions between neighboring agents [12], [17]. In [12], the authors identified the effectiveness of message passing GNN for solving the distributed power control and beamforming problems, and theoretically analyzed its permutation equivariance property, scalability, and generalization ability. Alternatively, the authors of [13] unfolded a power allocation enabled iterative weighted minimum mean squared error (WMMSE) algorithm with a distributed GNN architecture, which achieves higher robustness and generalizability in unseen scenarios. In reconfigurable intelligent surface (RIS) aided terahertz massive MIMO-NOMA networks, the authors of [14] integrated the graph neural network into distributed multi-agent deep reinforcement learning architecture to facilitate information interaction and coordination. Moreover, the authors of [15] learned a distributed heterogeneous GNN over wireless interference graph with a parameter sharing scheme, which enables more efficient scheduling than homogeneous GNNs.

## B. Motivations

The above-mentioned research contributions focused on the conventional multi-cell communications, whilst there is a paucity of investigations on the multi-cell cluster-free NOMA. Furthermore, the above optimization-based and learning-based distributed scheduling methods have their own demerits to deal with the distributed optimization in multi-cell scenarios.

- For conventional optimization-based distributed scheduling methods, they typically require a large number of iterations to converge [18], which is inapplicable for the tasks with low latency requirements. Moreover, when dealing with coupling mixed-integer optimization variables, the results are highly sensitive to initialized parameters, which should be carefully tuned for different scenarios. In a nutshell, the slow convergence and the manual searching of initialized parameters result in frequent information exchange among BSs, leading to high communication and computation overheads.
- For learning-based distributed scheduling methods, they can directly learn the mapping from agents' observations to the optimal solutions to overcome the parameter initialization dependence. Moreover, they can achieve real-time scheduling by learning desirable solutions through limited neural layers that require low-complexity calculations. However, conventional DNNs are awkward to exploit structural features and lacking generalization. Although GNNs can compensate for several weaknesses of DNNs, they still suffer predefined hyperparameters and fixed architectures that lead to inefficient distributed scheduling.

Against the above background, we propose a multi-cell cluster-free NOMA framework, where the coordinated beamforming and cluster-free SIC are jointly designed to mitigate interference as well as maximize the system sum rate. The joint optimization problem is formulated as a highly coupling and complex non-convex mixed-integer nonlinear programming (MINLP). To overcome the shortcomings of both conventional optimization-based and learning-based distributed scheduling methods, we propose a novel automated-learning graph neural network (AutoGNN), where the GNN architecture parameters, namely the number of GNN layers and the message embedding sizes between agents, can be automatically learned to alleviate the communication and computation burdens. By jointly training the GNN model weights and the architecture parameters, the proposed AutoGNN can enable a communication-efficient distributed scheduling paradigm.

## C. Contributions

The main contributions of this work can be summarized as follows.

- We propose a novel multi-cell cluster-free NOMA framework, which can flexibly mitigate both intra-cell and inter-cell interference via a joint cluster-free SIC and coordinated beamforming design. The objective function is formulated to maximize the system sum rate while satisfying the SIC decoding requirements and users' data rate constraints, which is a highly complex and coupling MINLP.
- We propose a novel communication-efficient learning architecture, namely AutoGNN, to realize distributed coordinated beamforming and cluster-free SIC optimization. Compared to conventional GNNs utilizing fixed architectures, the proposed AutoGNN can automatically learn the GNN network depths and message embedding sizes to alleviate the computation and information exchange burdens.
- We develop a bi-level AutoGNN learning algorithm to jointly train the GNN weights and architecture parameters to achieve intelligent distributed coordination, which can efficiently approximate the hypergradient in model training. Moreover, we analyze the upper bound of the approximation error and theoretically demonstrate that the bi-level AutoGNN learning algorithm can converge to a stationary point.
- Numerical results verify that the proposed multi-cell cluster-free NOMA framework outperforms conventional cluster-based NOMA framework in various scenarios. Moreover, compared to the conventional distributed ADMM and the fixed GNN algorithm, the proposed AutoGNN can significantly reduce computation and communication overheads without degrading the system performance.

The rest of this paper is organized as follows. Section II describes the downlink multi-cell cluster-free multi-antenna NOMA framework and formulates the sum rate maximization problem. A communication-efficient AutoGNN architecture is proposed in Section III. Next, a bi-level AutoGNN learning algorithm is developed in Section IV. In Section V, numerical results are presented to verify the effectiveness of the proposed framework and learning algorithms. Finally, Section VI concludes the paper.

## II. SYSTEM MODEL AND PROBLEM FORMULATION

### A. Downlink Multi-Cell Cluster-Free NOMA Framework

We propose a downlink coordinated multi-cell multi-antenna cluster-free NOMA framework, which consists of  $M$  BSs indexed by the set  $\mathcal{M} = \{1, 2, \dots, M\}$ . Each BS equips  $N_T$  antennas to serve  $K_m$  single-antenna users within its coverage, indexed by the set  $\mathcal{K}_m = \{1, 2, \dots, K_m\}$ .

Without loss of generality, we assume  $K = K_1 = K_2 = \dots = K_M$ . Note that the proposed framework can be employed in both underloaded ( $K \leq N_T$ ) and overloaded ( $K > N_T$ ) systems. Here, users served by each BS  $m$  are ordered according to the ascending order of their data channel gains. Define the transmit beamforming matrix of BS  $m$  as  $\mathbf{W}^m = [\mathbf{w}_1^m, \mathbf{w}_2^m, \dots, \mathbf{w}_K^m] \in \mathbb{C}^{N_T \times K}$ , where  $\mathbf{w}_k^m \in \mathbb{C}^{N_T \times 1}$  denotes the dedicated beamforming vector from BS  $m$  to user  $k$ .

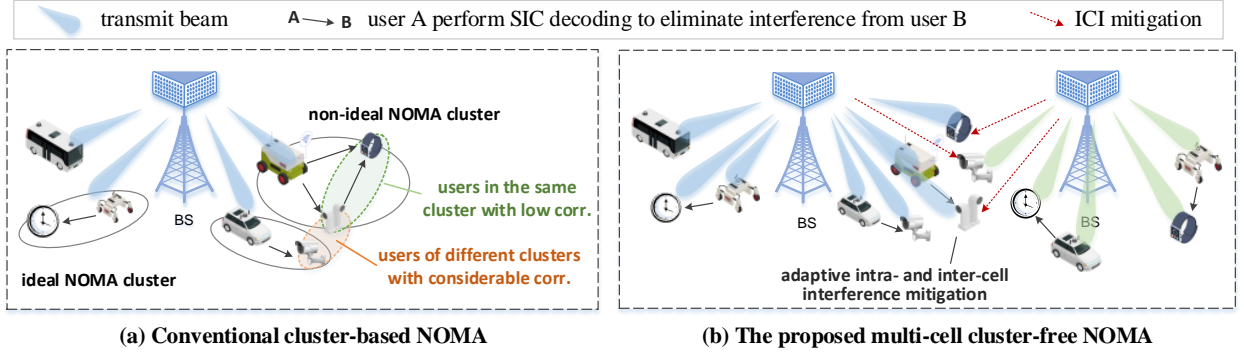


Fig. 1: Illustration of the proposed downlink multi-cell cluster-free NOMA framework.

The received signal at user  $k \in \mathcal{K}_m$  can be represented by

$$y_k^m = \underbrace{|\mathbf{h}_{mk}^m \mathbf{w}_k^m|^2 \sqrt{s_k^m}}_{\text{desired signal}} + \underbrace{\sum_{u \neq k} |\mathbf{h}_{mk}^m \mathbf{w}_u^m|^2 \sqrt{s_u^m}}_{\text{intra-cell interference}} + \underbrace{\sum_{n \neq m} \sum_{u \in \mathcal{K}_n} |\mathbf{h}_{mk}^n \mathbf{w}_u^n|^2 \sqrt{s_u^n}}_{\text{inter-cell interference}} + \underbrace{z_k^m}_{\text{noise}}, \quad \forall k \in \mathcal{K}_m, m \in \mathcal{M}, \quad (1)$$

where  $\mathbf{h}_{mk}^n \in \mathbb{C}^{1 \times N_T}$  denotes the channel from BS  $n$  to the  $k$ -th user served by BS  $m$ , and  $\mathbf{h}_{mk}^m \in \mathbb{C}^{1 \times N_T}$  signifies the channel from BS  $m$  to the  $k$ -th user served by BS  $m$ .

To reduce both the inter-cell and intra-cell interference, we jointly employ the multi-cell coordinated beamforming and the cluster-free SIC to transmit and decode users' signals, as shown in Fig. 1. Specifically, we introduce a cluster-free SIC scheme [4], where users can flexibly mitigate intra-cell interference unimpeded by predefined user clusters.

We specify the cluster-free SIC operations for each user  $k \in \mathcal{K}_m$  with a binary vector  $\beta_k^m = [\beta_{1k}^m, \beta_{2k}^m, \dots, \beta_{Kk}^m]^T$ , where  $\beta_{ik}^m \in \{0, 1\}$  indicates whether user  $i \in \mathcal{K}_m$  would carry out SIC to decode the signal of user  $k \in \mathcal{K}_m$ ,  $i \neq k$ , before decoding its own signal. The achievable rate of SIC decoding and downlink transmission can be modelled as follows.

1) *SIC decoding rate*: The interference  $\text{Intf}_{ik}^m(\beta^m, \mathbf{W})$  for user  $i$  to decode the signal of user  $k$ ,  $\forall i \neq k$ ,  $i, k \in \mathcal{K}_m$ , can be formulated as [4]

$$\begin{aligned} \text{Intf}_{ik}^m(\boldsymbol{\beta}^m, \mathbf{W}) = & \underbrace{\sum_{u < k} (1 - \beta_{iu}^m + \beta_{iu}^m \beta_{uk}^m) |\mathbf{h}_{mi}^m \mathbf{w}_u^m|^2}_{\text{intra-cell interference from weaker users}} + \underbrace{\sum_{u > k} (1 - \beta_{iu}^m \beta_{ku}^m) |\mathbf{h}_{mi}^m \mathbf{w}_u^m|^2}_{\text{intra-cell interference from stronger users}} \\ & + \text{ICI}_i^m(\mathbf{W}), \quad \forall i \neq k, \quad i, k \in \mathcal{K}_m, \quad m \in \mathcal{M}, \end{aligned} \quad (2)$$

where  $\boldsymbol{\beta}^m = [\beta_1^m, \beta_2^m, \dots, \beta_K^m]$  and  $\mathbf{W} = [\mathbf{W}^1, \mathbf{W}^2, \dots, \mathbf{W}^M]$  denote the stacked variables, and  $\text{ICI}_i^m(\boldsymbol{\beta}^m, \mathbf{W}) = \sum_{n \neq m} \sum_{u \in \mathcal{K}_n} |\mathbf{h}_{mi}^n \mathbf{w}_u^n|^2$  is the inter-cell interference (ICI) suffered by user  $i \in \mathcal{K}_m$ . Hence, when user  $i$  decoding user  $k$ 's signal, the received SINR  $\gamma_{ik}^m$  can be expressed as

$$\gamma_{ik}^m = \frac{|\mathbf{h}_{mi}^m \mathbf{w}_k^m|^2}{\text{Intf}_{ik}^m(\boldsymbol{\beta}^m, \mathbf{W}) + \sigma^2}, \quad \forall i \neq k, \quad i, k \in \mathcal{K}_m, \quad m \in \mathcal{M}. \quad (3)$$

Therefore, the corresponding SIC decoding rate can be derived as  $r_{ik}^m = \log_2(1 + \gamma_{ik}^m)$ .

2) *Transmission rate*: When user  $k$  decoding its own signal, the interference can be expressed as

$$\text{Intf}_{kk}^m(\boldsymbol{\beta}^m, \mathbf{W}) = \underbrace{\sum_{u \neq k} (1 - \beta_{ku}^m) |\mathbf{h}_{mk}^m \mathbf{w}_u^m|^2}_{\text{intra-cell interference after SIC}} + \underbrace{\text{ICI}_k^m(\mathbf{W})}_{\text{inter-cell interference}}, \quad \forall k \in \mathcal{K}_m, \quad m \in \mathcal{M}. \quad (4)$$

The corresponding transmission rate of user  $k$  can be computed by  $r_{kk}^m = \log_2(1 + \gamma_{kk}^m) = \log_2\left(1 + \frac{|\mathbf{h}_{mk}^m \mathbf{w}_k^m|^2}{\text{Intf}_{kk}^m(\boldsymbol{\beta}^m, \mathbf{W}) + \sigma^2}\right)$ .

To correctly decode the intended signal of user  $k$ , the received SINR for user  $i$  to decode user  $k$ 's signal should be larger than or equal to the received SINR of user  $k$  to decode its own signal,  $\forall \beta_{ik}^m = 1$  [19]. Owing to this SIC decoding constraint, the effective data rate  $R_k^m$  for each user  $k \in \mathcal{K}_m$  should be bounded by  $\beta_{ik}^m R_k^m \leq r_{ik}^m$ , which can be rearranged as

$$R_k^m = \min_{i \in \mathcal{K}_m} \left\{ \frac{1}{\beta_{ik}^m} r_{ik}^m \right\}, \quad \forall k \in \mathcal{K}_m, m \in \mathcal{M}. \quad (5)$$

## B. Problem Formulation

Based on the proposed multi-cell cluster-free NOMA framework, we aim to maximize the system sum rate through jointly optimizing coordinated beamforming  $\mathbf{W}$  and SIC operations  $\boldsymbol{\beta}$ , under the constraints of SIC decoding and users' minimal data rate requirements, which can be formulated as

$$\mathcal{P}_0 : \max_{\boldsymbol{\beta}, \mathbf{W}} \sum_{m \in \mathcal{M}} \sum_{k \in \mathcal{K}_m} \min_{i \in \mathcal{K}_m} \left\{ \frac{1}{\beta_{ik}^m} r_{ik}^m \right\} \quad (6a)$$

$$\text{s.t.} \quad R_k^m \geq R_k^{m, \min}, \quad \forall k \in \mathcal{K}_m, m \in \mathcal{M}, \quad (6b)$$

$$\sum_{k \in \mathcal{K}_m} \|\mathbf{w}_k^m\|^2 \leq P^{\max}, \quad \forall m \in \mathcal{M}, \quad (6c)$$

$$\beta_{ik}^m + \beta_{ki}^m \leq 1, \quad \forall i \neq k, i, k \in \mathcal{K}_m, m \in \mathcal{M}, \quad (6d)$$

$$\beta_{ik}^m \in \{0, 1\}, \forall i, k \in \mathcal{K}_m, m \in \mathcal{M}, \quad (6e)$$

where constraint (6b) guarantees the minimum data rate requirement  $R_k^{m,\min}$  of each user  $k \in \mathcal{K}_m$ , and (6c) ensures that the maximum transmit power of each BS does not exceed  $P^{\max}$ . Constraint (6d) indicates that user  $i$  and user  $k$ ,  $i \neq k$ , cannot mutually carry out SIC. Intuitively,  $\mathcal{P}_0$  is a highly coupling and complex non-convex MINLP, which is an NP-hard problem that is challenging to be optimally solved in a centralized way. To reduce computation complexity as well as relieve information exchange burdens, it is essential to obtain desirable solution of  $\mathcal{P}_0$  via efficient distributed scheduling methods.

### III. COMMUNICATION-EFFICIENT AUTOGNN ARCHITECTURE

In this section, we propose a novel AutoGNN architecture to achieve communication-efficient distributed scheduling in multi-cell cluster-free NOMA networks. We first model the proposed multi-cell cluster-free NOMA framework as a distributed communication graph. Thereafter, a novel communication-efficient AutoGNN architecture is proposed to overcome the inefficiency of the conventional message passing GNN built on fixed architectures.

#### A. Distributed Communication Graph Model

The proposed multi-cell cluster-free NOMA framework can be modelled as a distributed communication graph  $\mathcal{G}$ , denoted by  $\mathcal{G} = \{\mathcal{M}, \mathcal{E}, \mathbf{O}, \mathbf{X}\}$ .  $\mathcal{G}$  is a directed graph, where all the BSs are modelled into a set of nodes  $\mathcal{M}$ , and the interplay effects among BSs are represented by a set of edge  $\mathcal{E}$ . Let  $E_{mn} \in \mathcal{E}$  denote the edge from node  $m$  to node  $n$ , which signifies an outbound edge from node  $m$  and an inbound edge to node  $n$ . Let  $\mathcal{N}_m^{\text{out}}$  ( $\mathcal{N}_m^{\text{in}}$ ) denote the sets of nodes that connect with node  $m$  through an outbound (inbound) edge of node  $m$ , and  $N_m^{\text{out}}$  and  $N_m^{\text{in}}$  are the cardinality of sets  $\mathcal{N}_m^{\text{out}}$  and  $\mathcal{N}_m^{\text{in}}$ , respectively. Moreover,  $\mathbf{O} = [\mathbf{O}_1, \mathbf{O}_2, \dots, \mathbf{O}_M]$  and  $\mathbf{X} = [\mathbf{X}_1, \mathbf{X}_2, \dots, \mathbf{X}_M]$  denote the joint observations and hidden states, where  $\mathbf{O}_m$  and  $\mathbf{X}_m$  denote the local observation and local hidden states at BS  $m$ , respectively. The local observation  $\mathbf{O}_m$  is partially observable by BS  $m$ , which consists of the node feature  $\mathbf{O}_m^{\text{N}}$  and the edge feature  $\{\mathbf{O}_{mn}^{\text{E}}\}_{n \in \mathcal{N}_m^{\text{out}}}$ .

Based on the directed graph model, we can straightforwardly model the data channels from each BS  $m$  to its serving users as its node feature, and depict the interference channels from BS  $m$  to the device served by other BSs as its edge features, which can be expressed as

$$\mathbf{O}_m^{\text{N}} = \mathbf{H}_{mm} = [\{\mathbf{h}_{mk}^m\}_{k \in \mathcal{K}_m}], \forall m \in \mathcal{M}, \quad (7)$$



$$\mathbf{O}_{mn}^E = \mathbf{H}_{mn} = [\{\mathbf{h}_{nk}^m\}_{k \in \mathcal{K}^n}], \quad \forall m \neq n, n \in \mathcal{N}_m^{\text{out}}, \quad (8)$$

where  $\mathbf{H}_{mn} \in \mathbb{C}^{N_T \times K}$  collects the data channels from BS  $m$  to its serving users, and  $\mathbf{H}_{mn} \in \mathbb{C}^{N_T \times K}$  stacks the interference channels from BS  $m$  to users served by the neighboring BS  $n \in \mathcal{N}_m^{\text{out}}$ , respectively. Moreover, the local hidden states at each BS  $m$  can be initialized by the input node feature, i.e.,  $\mathbf{X}_m^0 = \mathbf{O}_m^N$ . Based on the distributed communication graph model, we introduce the conventional message passing GNN and the proposed AutoGNN architecture as follows.

### B. Conventional Message Passing GNN

Conventional message passing GNN [12] can eliminate the parameter initialization dependence and avoid the slow convergence of conventional iterative optimization algorithms. Following the principle of DNNs, GNN exploits a multi-layer structure. Define  $L$  as the number of GNN layers, and  $\boldsymbol{\theta} = [\boldsymbol{\theta}^{(1)}, \boldsymbol{\theta}^{(2)}, \dots, \boldsymbol{\theta}^{(L)}]$  as the set of model weights of the entire GNN. Each GNN layer  $l$  includes a distributed message passing process to achieve agents' coordination, which consists of three steps, namely the message embedding, the message aggregation, and the message combination. The detailed process can be illustrated as follows.

**(i) Message embedding.** At each layer  $l$ , agent  $m$  embeds the local hidden state  $\mathbf{X}_m^{(l)}$  and the outbound edge feature  $\mathbf{O}_{mn}^E$  to obtain a message vector  $\mathbf{u}_{mn}^{(l)} = [u_{mn1}^{(l)}, u_{mn2}^{(l)}, \dots, u_{mnD^E}^{(l)}] \in \mathbb{R}^{D^E \times 1}$ , where  $D^E$  represents the embedding size of  $\mathbf{u}_{mn}^{(l)}$ . Thereafter, agent  $m$  would send the outbound embedded message  $\mathbf{u}_{mn}^{(l)}$  to agent  $n \in \mathcal{N}_m^{\text{out}}$ , and then receives the inbound embedded message  $\mathbf{u}_{nm}^{(l)}$  from agent  $n \in \mathcal{N}_m^{\text{in}}$ . The embedded message  $\mathbf{u}_{mn}^{(l)}$  from agent  $m$  to agent  $n$  can be obtained by the local encoder  $\phi_E^l$  as

$$\mathbf{u}_{mn}^{(l)} = \phi_E^l \left( \mathbf{X}_m^{(l-1)}, \mathbf{O}_{mn}^E; \boldsymbol{\theta}_E^{(l)} \right), \quad \forall n \in \mathcal{N}_m^{\text{out}}, \quad (9)$$

where  $\phi_E^l(\cdot; \boldsymbol{\theta}_E^{(l)})$  denotes the local embedding function at layer  $l$ , which is implemented as a multi-layer perceptrons (MLPs) parameterized by  $\boldsymbol{\theta}_E^{(l)}$ .

**(ii) Message aggregation.** After receiving the embedded messages  $\mathbf{u}_{mn}^{(l)}$  from neighboring agents  $n \in \mathcal{N}_m^{\text{in}}$ , agent  $m$  can aggregate the messages  $\mathbf{u}_{mn}^{(l)}, \forall n \in \mathcal{N}_m^{\text{in}}$ , as

$$\bar{\mathbf{u}}_m^{(l)} = \phi_A \left( \{\mathbf{u}_{mn}^{(l)}\}_{\forall n \in \mathcal{N}_m^{\text{in}}}; \boldsymbol{\theta}_A^{(l)} \right), \quad (10)$$

where  $\phi_A$  denotes a permutation-invariant function, such as  $\text{mean}(\cdot)$ ,  $\text{sum}(\cdot)$ , and  $\text{max}(\cdot)$ .

**(iii) Message combination.** Given the combination function  $\phi_C$ , the local hidden state at agent  $m$  can be updated by

$$\mathbf{X}_m^{(l)} = \psi_{\text{C}} \left( \mathbf{X}_m^{(l-1)}, \bar{\mathbf{u}}_m^{(l)}; \boldsymbol{\theta}_{\text{C}}^{(l)} \right). \quad (11)$$

Define the optimization variables predicted by GNN as  $\mathbf{Z} = [\mathbf{Z}_1, \mathbf{Z}_2, \dots, \mathbf{Z}_M]$ , with  $\mathbf{Z}_m = \{\beta^m, \tilde{\beta}^m, \mathbf{W}^m\}$  being the local optimization variables at BS  $m$ . The optimization variables can be obtained via a fully connected (FC) layer, which can be expressed as

$$\mathbf{Z}_m = \psi_{\text{FC}}(\mathbf{O}_m^N, \mathbf{X}_m^{(L)}), \quad (12)$$

where  $\varphi_{\text{FC}}(\cdot)$  denotes the FC layer function.

### C. Communication-Efficient AutoGNN Architecture

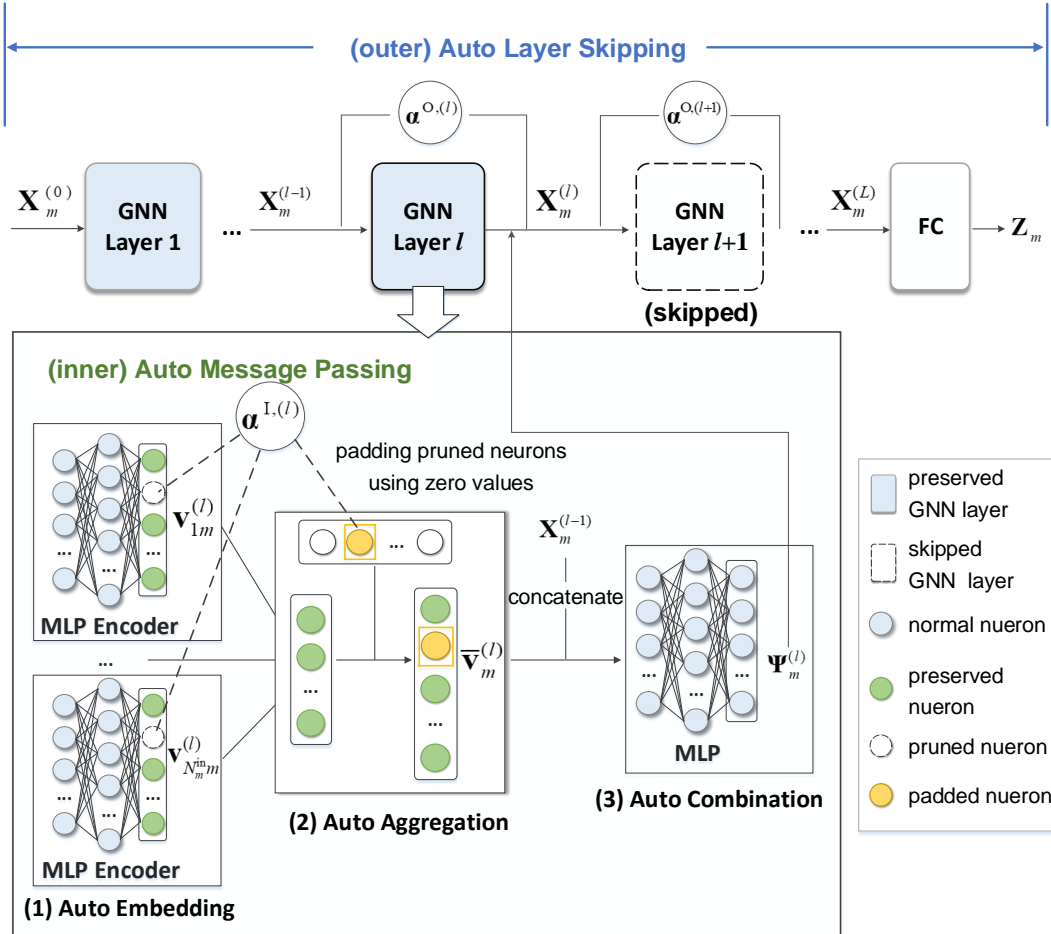


Fig. 2: Illustration of the proposed AutoGNN architecture.

To accommodate various communication scenarios, the static GNN architectures should be artificially and empirically designed for different environments. However, it is generally time-consuming, laborious, and error-prone to search for the optimal neural network architecture and hyperparameters. Neural architecture searching (NAS) [16], [20]–[22] has been proposed as

a promising automated machine learning (AutoML) paradigm to automate the neural network design. Inspired by AutoML, we propose a novel AutoGNN architecture, which automates the architecture parameters and structure designs of the message passing GNN.

As shown in Fig. 2, the proposed AutoGNN architecture has a dual-loop auto-learned structure, which consists of an inner auto message passing module and an outer auto layer skipping module. These auto-learned modules can adaptively configure the network widths (embedding sizes) of the inner MLP encoders and the network depths (the number of layers) of the GNN.

*1) Auto Message Passing Module:* The inner auto message passing module for each GNN layer consists of three steps, namely the auto message embedding, the auto message aggregation, and the auto message combination.

**(i) Auto message embedding.** The high-dimensional node/edge features are embedded through the local encoder, and agents only need to exchange the low-dimensional embedded messages for achieving coordination. Different from the conventional GNN architecture that utilizes a predefined embedding size, the auto message passing module enables an automated learning-based control of message embedding size for each GNN layer. Therefore, it can fully exploit the potential of deep learning to efficiently reduce the dimensions of the embedded messages. In detail, the auto message passing module would selectively cutting unnecessary output neurons and dynamically determine the network width of the inner MLP.

Without loss of generality, we implement the local encoder  $\phi_E^l$  for message embedding as an inner MLP at GNN layer  $l$ . We define the binary vector  $\alpha^{I,(l)} = [\alpha_1^{I,(l)}, \alpha_2^{I,(l)}, \dots, \alpha_{D^E}^{I,(l)}] \in \mathbb{R}^{1 \times D^E}$  to specify the selective pruning of neurons, where  $\alpha_i^{I,(l)} = 1$  if the  $i$ -th neuron is reserved, and  $\alpha_i^{I,(l)} = 0$  otherwise. In order to carry out the message aggregation and combination, the sizes of the adapted messages received by each agent should be consistent with the input size of the combination function  $\psi_C^l(\cdot)$ . In this way, each agent would fill in the pruned neurons with zero values. Furthermore, we assume that no neurons would be pruned at the first GNN layer.

To make the binary vector  $\alpha^{I,(l)}$  learnable, we further introduce the auxiliary vector  $\tilde{\alpha}^{I,(l)} \in \mathbb{R}^{D^E \times 1}$ , which satisfies

$$\tilde{\alpha}^{I,(l)} + \alpha^{I,(l)} = \mathbf{1}, \quad \forall l \in \mathcal{L}. \quad (13)$$

Then, the resulting message  $\mathbf{v}_{mn}^{(l)}$  received by agent  $n$  from agent  $m \in \mathcal{N}_n^{\text{in}}$  can be modelled as

$$\mathbf{v}_{mn}^{(l)} = \begin{cases} \phi_E^l(\mathbf{O}_m^N, \mathbf{O}_{mn}^E), & l=1, \\ (\alpha^{I,(l)})^T \phi_E^l(\mathbf{X}_m^{(l-1)}, \mathbf{O}_{mn}^E), & l>1. \end{cases} \quad (14)$$

(ii) **Auto message aggregation.** Using the flexibly embedded messages  $\mathbf{v}_{mn}^{(l)}$  given in (14) from all the neighboring agents  $m \in \mathcal{N}_n^{\text{in}}$ , agent  $n$  aggregates the messages using a permutation-equivalent aggregation function  $\phi_A(\cdot)$ . Therefore, the aggregated features  $\bar{\mathbf{v}}_n^{(l)}$  at agent  $n$  can be written as

$$\bar{\mathbf{v}}_n^{(l)} = \phi_A \left( \left\{ \mathbf{v}_{mn}^{(l)} \right\}_{m \in \mathcal{N}_n^{\text{in}}} \right), \forall n \in \mathcal{M}, l \in \mathcal{L}. \quad (15)$$

(iii) **Auto message combination.** To update the hidden state variables at layer  $l$ , each agent  $m$  can combine the aggregated feature  $\bar{\mathbf{v}}_m^l$  with the previous hidden state  $\mathbf{X}_m^{(l-1)}$  through the combination function  $\psi_C^l(\cdot)$ , as

$$\Psi_m^{(l)} = \psi_C^l \left( \mathbf{X}_m^{(l-1)}, \bar{\mathbf{v}}_m^{(l)} \right), \forall m \in \mathcal{M}, l \in \mathcal{L}. \quad (16)$$

2) *Auto Layer Skipping Module:* Different from the conventional GNN architecture that has fixed number of layers, the outer auto layer skipping module learns to adaptively skip insignificant GNN layers and avoid unnecessary communication rounds to reduce both computation complexity and communication overheads.

Define a binary vector set of the skipper layer as  $\alpha^O = [\alpha^{O,(l)}, \alpha^{O,(l)}, \dots, \alpha^{O,(L)}]^T$ , where  $\alpha^{O,(l)} = 0$  means the  $l$ -th GNN layer is skipped, and  $\alpha^{O,(l)} = 1$  otherwise. Similarly, we introduce  $\tilde{\alpha}^O$  to make the binary vector  $\alpha^O$  learnable, which satisfies

$$\tilde{\alpha}^O + \alpha^O = 1. \quad (17)$$

As a result, the hidden state at each GNN layer  $l$  can be updated as

$$\mathbf{X}_m^{(l)} = \alpha^{O,(l)} \Psi_m^{(l)} + \tilde{\alpha}^{O,(l)} \mathbf{X}_m^{(l-1)}, \forall m \in \mathcal{M}, l \in \mathcal{L}. \quad (18)$$

Eventually, the optimization variables can be predicted by the FC layer  $\varphi_{\text{FC}}(\cdot)$  as (12).

---

**Algorithm 1** Distributed Scheduling Based on the proposed AutoGNN architecture

---

**Input:** The GNN weights  $\theta$ , architecture parameters  $\alpha$ , and the channel samples.

- 1: **for** each GNN layer  $l \in \mathcal{L}$  **do**
  - 2:   **for** each BS (agent)  $m \in \mathcal{M}$  **do**
  - 3:     **if**  $\alpha^{O,(l)} = 0$  **then**
  - 4:       Skip the current GNN layer.
  - 5:     **else**
  - 6:       For each neighboring agent  $n \in \mathcal{N}_m^{\text{in}}$ , agent  $m$  encodes the local information into the embedded message  $\mathbf{v}_{mn}^{(l)}$  based on (14) and send  $\mathbf{v}_{mn}^{(l)}$  to agent  $n$ .
  - 7:       Each agent  $m$  aggregate the received messages  $\mathbf{v}_{nm}^{(l)}$ ,  $\forall n \in \mathcal{N}_m^{\text{out}}$  using (15), and update the local hidden state using (16) and (18).
  - 8:     **end if**
  - 9:   **end for**
  - 10: **end for**
  - 11: Predict the local optimization variables at each BS  $m$  using (12).
-

The distributed scheduling based on the proposed AutoGNN architecture can be summarized in Algorithm 1.

#### IV. BI-LEVEL AUTOGNN LEARNING ALGORITHM

To achieve efficient scheduling based on the proposed AutoGNN architecture, we should jointly train the GNN weights  $\theta$  and architecture parameters  $\alpha$  to predict desirable solutions. In this section, we first formulate the model training of AutoGNN as a bi-level programming, where the GNN weights are optimized in the lower level to maximize the training rates, whilst the architecture parameters are optimized in the upper level to maximize the validation rate. Thereafter, a bi-level AutoGNN learning algorithm is developed to efficiently calculate hypergradient for the AutoGNN model training.

##### A. Penalty-Based Bi-Level Programming for AutoGNN Learning

Based on the proposed AutoGNN architecture, the achievable data rate of user  $k \in \mathcal{K}^m$  in (5) can be rewritten as

$$R_k^m(\theta, \alpha) = \min_{i \in \mathcal{K}^m} \left\{ \beta_{ik}^m(\theta, \alpha) r_{ik}^m(\theta, \alpha) + (1 - \beta_{ik}^m(\theta, \alpha)) r_{kk}^m(\theta, \alpha) \right\}, \quad \forall k \in \mathcal{K}_m, \quad m \in \mathcal{M}. \quad (19)$$

where  $\alpha = \{\alpha^O, \tilde{\alpha}^O, \alpha^I, \tilde{\alpha}^I\}$  is the combined architecture parameter vector. Then, the achievable system sum rate of the cluster-free NOMA networks can be formulated as  $R(\theta, \alpha) = \sum_{m \in \mathcal{M}} \sum_{k \in \mathcal{K}^m} R_k^m(\theta, \alpha)$ .

Thereafter, the joint learning of architecture parameters  $\alpha$  and GNN parameters  $\theta$  problem can be formulated as a bi-level programming. In the inner loop, we train GNN parameters  $\theta$  to maximize the training sum rate under fixed  $\alpha$ . In the outer loop, the optimal architecture parameters  $\alpha$  are searched to maximize the validation sum rate. Let  $R(\theta, \alpha)$  and  $\hat{R}_v(\theta, \alpha)$  be the achieved sum rate during training and validation, respectively. The bi-level joint optimization problem can be written as

$$\min_{\alpha} -\hat{R}_v(\theta^*(\alpha), \alpha) \quad (20a)$$

$$\text{s.t. } \theta^*(\alpha) = \arg \min_{\theta} -R(\theta, \alpha), \quad (20b)$$

$$\alpha_i^{I,(l)}, \tilde{\alpha}_i^{I,(l)} \in \{0, 1\}, \quad \forall 1 \leq i \leq D^E, l \in \mathcal{L}, \quad (20c)$$

$$\alpha^{O,(l)}, \tilde{\alpha}^{O,(l)} \in \{0, 1\}, \quad \forall l \in \mathcal{L}, \quad (20d)$$

$$\beta_{ik}^m(\theta, \alpha), \zeta_{ik}^m(\theta, \alpha) \in \{0, 1\}, \quad (20e)$$

$$\sum_{k \in \mathcal{K}_m} \|\mathbf{w}_k^m(\boldsymbol{\theta}, \boldsymbol{\alpha})\|^2 \leq P^{\max}, \quad \forall m \in \mathcal{M}, \quad (20f)$$

$$\beta_{ik}^m(\boldsymbol{\theta}, \boldsymbol{\alpha}) + \beta_{ki}^m(\boldsymbol{\theta}, \boldsymbol{\alpha}) + \zeta_{ik}^m(\boldsymbol{\theta}, \boldsymbol{\alpha}) = 1, \quad \forall i \neq k, \quad (20g)$$

$$(13), (17). \quad (20h)$$

1) *Penalty Function:* We invoke the penalty method to deal with the binary constraints (20c) and (20d), which can be equivalently transferred into

$$\alpha_i^{I,(l)} \tilde{\alpha}_i^{I,(l)} = 0, \quad \forall 1 \leq i \leq D^E, l \in \mathcal{L}, \quad (21)$$

$$\alpha^{O,(l)} \tilde{\alpha}^{O,(l)} = 0, \quad \forall l \in \mathcal{L}. \quad (22)$$

Similarly, the binary constraints (20e) can be equivalently recast as

$$\beta_{ik}^m(\boldsymbol{\theta}, \boldsymbol{\alpha}) (1 - \beta_{ik}^m(\boldsymbol{\theta}, \boldsymbol{\alpha})) = 0, \quad \zeta_{ik}^m(\boldsymbol{\theta}, \boldsymbol{\alpha}) (1 - \zeta_{ik}^m(\boldsymbol{\theta}, \boldsymbol{\alpha})) = 0, \quad \forall i \neq k, \quad i, k \in \mathcal{K}_m, \quad m \in \mathcal{M}. \quad (23)$$

Based on the penalty method, we formulate the penalty function  $h_\alpha(\boldsymbol{\alpha}, \tilde{\boldsymbol{\alpha}})$  to handle the equality constraints (21) and (22), which is defined as

$$h_\alpha(\boldsymbol{\alpha}) = \sum_{l \in \mathcal{L}} (\boldsymbol{\alpha}^{I,(l)})^T \tilde{\boldsymbol{\alpha}}^{I,(l)} + (\boldsymbol{\alpha}^O)^T \tilde{\boldsymbol{\alpha}}^O. \quad (24)$$

Meanwhile, we define the penalty function  $h_\beta(\boldsymbol{\alpha}, \tilde{\boldsymbol{\alpha}})$  to tackle the equality constraints (23) as

$$h_\beta(\boldsymbol{\theta}, \boldsymbol{\alpha}) = \sum_{m \in \mathcal{M}} (1 - \text{vec}(\boldsymbol{\beta}^m(\boldsymbol{\theta}, \boldsymbol{\alpha})))^T \text{vec}(\boldsymbol{\beta}^m(\boldsymbol{\theta}, \boldsymbol{\alpha})) + \sum_{m \in \mathcal{M}} (1 - \text{vec}(\boldsymbol{\zeta}^m(\boldsymbol{\theta}, \boldsymbol{\alpha})))^T \text{vec}(\boldsymbol{\zeta}^m(\boldsymbol{\theta}, \boldsymbol{\alpha})). \quad (25)$$

Therefore, we can formulate the penalty-based loss function of the AutoGNN as

$$\mathcal{L}(\boldsymbol{\theta}, \boldsymbol{\alpha}) = - \sum_{m \in \mathcal{M}} R^m(\boldsymbol{\theta}, \boldsymbol{\alpha}) + \lambda_\alpha h_\alpha(\boldsymbol{\alpha}) + \lambda_\beta h_\beta(\boldsymbol{\theta}, \boldsymbol{\alpha}) + \eta v(\boldsymbol{\theta}, \boldsymbol{\alpha}), \quad (26)$$

where  $\lambda_\alpha$  and  $\lambda_\beta$  are the penalty factors corresponding to penalty functions (24) and (25). Moreover,  $v(\boldsymbol{\theta}, \boldsymbol{\alpha}) = [R^{\min} - R_k^m(\boldsymbol{\theta}, \boldsymbol{\alpha})]^+$  denotes the rate constraint violation, and  $\eta > 0$  punishes the rate constraint violation. Let  $\mathcal{L}_v(\boldsymbol{\theta}, \boldsymbol{\alpha})$  and  $\mathcal{L}(\boldsymbol{\theta}, \boldsymbol{\alpha})$  indicate the validation and training losses calculating over validation and training datasets, respectively. Then, the bi-level programming (20) can be recast as

$$\min_{\boldsymbol{\alpha}} \mathcal{L}_v(\boldsymbol{\theta}^*(\boldsymbol{\alpha}), \boldsymbol{\alpha}) \quad (27a)$$

$$\text{s.t. } \boldsymbol{\theta}^*(\boldsymbol{\alpha}) = \arg \min_{\boldsymbol{\theta}} \mathcal{L}(\boldsymbol{\theta}, \boldsymbol{\alpha}), \quad (27b)$$

$$\sum_{k \in \mathcal{K}_m} \|\mathbf{w}_k^m(\boldsymbol{\theta}, \boldsymbol{\alpha})\|^2 \leq P^{\max}, \quad \forall m \in \mathcal{M}, \quad (27c)$$

$$\beta_{ik}^m(\boldsymbol{\theta}, \boldsymbol{\alpha}) + \beta_{ki}^m(\boldsymbol{\theta}, \boldsymbol{\alpha}) + \zeta_{ik}^m(\boldsymbol{\theta}, \boldsymbol{\alpha}) = 1, \quad \forall i \neq k, \quad (27d)$$

$$(13), (17). \quad (27e)$$

2) *Constraint guarantees:* The transmission power constraints (27c) can be directly ensured by projecting the decision variable  $\mathbf{W}^m = \mathbf{W}^m(\boldsymbol{\theta}, \boldsymbol{\alpha})$  onto the feasible region as

$$\mathbf{W}^m := \Pi_{\mathcal{W}} \{ \mathbf{W}^m \} = \begin{cases} \mathbf{W}^m, & \text{if } \sum_{k \in \mathcal{K}^m} \mathbf{w}_k^m \leq P^{\max}, \\ \frac{\mathbf{W}^m \sqrt{P^{\max}}}{\|\mathbf{W}^m\|}, & \text{otherwise.} \end{cases} \quad (28)$$

Moreover, we introduce the softmax activation function to handle the equality constraints (13), (17), and (27d). Given the output variables  $\mathbf{x}_1, \mathbf{x}_2, \dots, \mathbf{x}_N$  predicted by the final GNN layer, the softmax activation function  $\text{Softmax}(\cdot)$  over  $\mathbf{x}_1, \mathbf{x}_2, \dots, \mathbf{x}_N$  can be defined as

$$\text{Softmax}([\mathbf{x}_1, \mathbf{x}_2, \dots, \mathbf{x}_N]) \triangleq \left[ \frac{e^{\mathbf{x}_1}}{\sum_n e^{\mathbf{x}_n}}, \frac{e^{\mathbf{x}_2}}{\sum_n e^{\mathbf{x}_n}}, \dots, \frac{e^{\mathbf{x}_N}}{\sum_n e^{\mathbf{x}_n}} \right]. \quad (29)$$

Based on the above definition, we can observe that the equality constraint  $\sum_{n=1}^N \mathbf{x}_n = 1$  can be stringently guaranteed by simply normalizing the output variables via the softmax activation function (29), i.e.,

$$[\mathbf{x}_1, \mathbf{x}_2, \dots, \mathbf{x}_N] := \text{Softmax}([\mathbf{x}_1, \mathbf{x}_2, \dots, \mathbf{x}_N]). \quad (30)$$

Therefore, the equality constraints (13), (17), and (27d) can be enforced by directly normalizing the hyper module parameter  $\boldsymbol{\alpha}$  and the SIC operation vector  $\boldsymbol{\beta}$  by

$$[\boldsymbol{\alpha}^{\text{I},(l)}, \tilde{\boldsymbol{\alpha}}^{\text{I},(l)}] := \text{Softmax}([\boldsymbol{\alpha}^{\text{I},(l)}, \tilde{\boldsymbol{\alpha}}^{\text{I},(l)}]), \quad (31)$$

$$[\boldsymbol{\alpha}^{\text{O}}, \tilde{\boldsymbol{\alpha}}^{\text{O}}] := \text{Softmax}([\boldsymbol{\alpha}^{\text{O}}, \tilde{\boldsymbol{\alpha}}^{\text{O}}]), \quad (32)$$

$$[\beta_{ik}^m, \beta_{ki}^m, \zeta_{ik}^m] := \text{Softmax}([\beta_{ik}^m(\boldsymbol{\theta}, \boldsymbol{\alpha}), \beta_{ki}^m(\boldsymbol{\theta}, \boldsymbol{\alpha}), \zeta_{ik}^m(\boldsymbol{\theta}, \boldsymbol{\alpha})]). \quad (33)$$

By ensuring constraints (27c) - (27e) through the operations (28) and (31) - (33), we can directly deal with the following unconstrained penalty-based bi-level programming as

$$\min_{\boldsymbol{\alpha}} \mathcal{L}_v(\boldsymbol{\theta}^*(\boldsymbol{\alpha}), \boldsymbol{\alpha}) \quad (34a)$$

$$\text{s.t. } \boldsymbol{\theta}^*(\boldsymbol{\alpha}) = \arg \min_{\boldsymbol{\theta}} \mathcal{L}(\boldsymbol{\theta}, \boldsymbol{\alpha}). \quad (34b)$$

### B. Bi-Level AutoGNN Learning Algorithm

In this paper, we refer the gradients of the outer-loop loss function with respect to architecture parameters  $\boldsymbol{\alpha}$  as hypergradient [22], [23]. For the sake of expression, we denote the optimal model weights obtained in the inner-loop optimization by  $\boldsymbol{\Theta} \triangleq \boldsymbol{\theta}^* = \boldsymbol{\theta}^*(\boldsymbol{\alpha})$ , which is a function of  $\boldsymbol{\alpha}$  as defined in (34b). Based on the chain rule, the hypergradient consisting of the direct and indirect components can be derived by

$$\nabla_{\boldsymbol{\alpha}} \mathcal{L}_v = \underbrace{\frac{\partial \mathcal{L}_v(\boldsymbol{\Theta}, \boldsymbol{\alpha})}{\partial \boldsymbol{\alpha}}}_{\text{direct gradient}} + \underbrace{\frac{\partial \mathcal{L}_v(\boldsymbol{\Theta}, \boldsymbol{\alpha})}{\partial \boldsymbol{\Theta}} \overbrace{\nabla_{\boldsymbol{\alpha}} \boldsymbol{\theta}^*(\boldsymbol{\alpha})}^{\text{best-response Jacobian}}}_{\text{indirect gradient}}. \quad (35)$$

Here, the direct gradient  $\frac{\partial \mathcal{L}_v(\Theta, \alpha)}{\partial \alpha}$  can be directly computed. Hence, the main difficulty to calculate (35) lies in the computation of the indirect gradient, where the best-response Jacobian  $\nabla_{\alpha} \theta^*(\alpha)$  should be evaluated using the local optimum  $\theta^*$  from the inner loop. For simplicity, we denote  $\mathcal{L}_v(\Theta, \alpha) = \mathcal{L}_v$  and  $\mathcal{L}(\theta, \alpha) = \mathcal{L}$  hereinafter. The hypergradient calculation is discussed in the following.

1) *Unrolling-based hypergradient*: Generally, the hypergradient defined in (35) can be computed by the reverse-mode unrolling method [25], [26], which takes large enough gradient descent steps in the inner loop under given  $\alpha$  to estimate the optimal  $\theta^*(\alpha)$ , and thus compute the best-response Jacobian  $\nabla_{\alpha} \theta^*(\alpha)$  in (35). Specifically, given an initial point  $\theta_0$ , the update rule of the GNN weights based on the gradient descent at the  $t$ -th inner-loop step can be written as

$$\theta_t = \Phi(\theta_{t-1}, \alpha), \quad (36)$$

where  $\Phi(\theta_{t-1}, \alpha) = \theta_{t-1} - \kappa \nabla_{\theta} \mathcal{L}(\theta_{t-1}, \alpha)$ . Let  $T$  be the total number of inner-loop optimization iterations, we have  $\theta^*(\alpha) = \Phi(\theta_{T-1}, \alpha) = \Phi(\Phi(\dots \Phi(\theta_0, \alpha) \dots), \alpha)$ . Based on the chain rule, the hypergradient can be recursively derived as

$$\nabla_{\alpha} \mathcal{L}^{\text{Rev}} = \frac{\partial \mathcal{L}_v}{\partial \alpha} + \frac{\mathcal{L}_v}{\partial \Theta} \left( \sum_{t=0}^T V_t Q_{t+1} \dots Q_T \right), \quad (37)$$

where  $Q_t = \nabla_{\theta} \Phi(\theta_{t-1}, \alpha)$  and  $V_t = \nabla_{\alpha} \Phi(\theta_{t-1}, \alpha)$ .

From (37), it is intuitive that all the intermediate GNN gradients of  $T$  inner-loop steps should be recorded. To reduce the memory cost, the truncated back propagation was proposed in [26], which approximately computes the hypergradient by only storing the intermediate gradients of the last  $\tau$  iterations in the inner loop ( $\tau \ll T$ ), i.e.,

$$\nabla_{\alpha} \hat{\mathcal{L}}_{\tau}^{\text{Trun}} = \frac{\partial \mathcal{L}_v}{\partial \alpha} + \frac{\partial \mathcal{L}_v}{\partial \Theta} \sum_{t=T-\tau+1}^T V_t Q_{t+1} \dots Q_T. \quad (38)$$

Nevertheless, this method still suffers unaffordable memory costs when training a large number of neural network parameters, which leads to the impracticability and inapplicability for deep learning. To achieve cost-efficient computation, we approximate the hypergradient using implicit function theorem (IFT) [23], [24], which can efficiently compute the hypergradient without recording any intermediate gradients, as analyzed as follows.

2) *Implicit hypergradient*: We invoke IFT to equivalently transform the unrolling-based hypergradient. To begin with, we introduce the following assumptions for the inner and outer loss functions, which are commonly considered in differentiable bi-level learning algorithms [22], [25], [27].



**Assumption 1.** The non-convex inner-loop function  $\mathcal{L}(\boldsymbol{\theta}, \boldsymbol{\alpha})$  has the following properties:

- (i) Function  $\boldsymbol{\theta}^*(\boldsymbol{\alpha})$  is Lipschitz continuous with constant  $L^\alpha > 0$ , and has Lipschitz-continuous gradient with constant  $\tilde{L}^\alpha > 0$ .
- (ii) Function  $\mathcal{L}(\boldsymbol{\theta}, \boldsymbol{\alpha})$  is twice differentiable and has Lipschitz-continuous gradient w.r.t.  $\boldsymbol{\theta}$  with constant  $\tilde{L}^\theta > 0$ , i.e.,  $\left\| \frac{\partial \mathcal{L}}{\partial \boldsymbol{\theta}_0} - \frac{\partial \mathcal{L}}{\partial \boldsymbol{\theta}_1} \right\| \leq \tilde{L}^\theta \|\boldsymbol{\theta}_0 - \boldsymbol{\theta}_1\|$ . Moreover, for some constant  $C^{\theta\alpha} > 0$ ,  $\left\| \frac{\partial^2 \mathcal{L}}{\partial \boldsymbol{\alpha} \partial \boldsymbol{\theta}} \right\| \leq C^{\theta\alpha}$ .
- (iii)  $\mathcal{L}(\boldsymbol{\theta}, \boldsymbol{\alpha})$  is locally strongly  $\mu$ -convex with respect to  $\boldsymbol{\theta}$  around  $\boldsymbol{\theta}^*(\boldsymbol{\alpha})$ , meaning that the Hessian matrix  $\frac{\partial^2 \mathcal{L}}{\partial \boldsymbol{\theta} \partial \boldsymbol{\theta}} \succeq \mu \mathbf{I}$  over a local  $l_2$  ball  $\mathcal{B}_\varsigma(\boldsymbol{\theta}) := \{\boldsymbol{\theta} \mid \|\boldsymbol{\theta} - \boldsymbol{\theta}^*(\boldsymbol{\alpha})\| \leq \varsigma \|\boldsymbol{\theta}\|\}$  surrounding  $\boldsymbol{\theta}^*(\boldsymbol{\alpha})$ .

**Assumption 2.** The non-convex outer-loop function  $\mathcal{L}_v(\boldsymbol{\Theta}, \boldsymbol{\alpha})$  is Lipschitz continuous with respect to  $\boldsymbol{\Theta}$  and  $\boldsymbol{\alpha}$  with constants  $L_v^\Theta > 0$  and  $L_v^\alpha > 0$ , and has Lipschitz-continuous gradient with constants  $\tilde{L}_v^\Theta > 0$  and  $\tilde{L}_v^\alpha > 0$ . Moreover, for some constant  $C_v^\theta$ ,  $\left\| \frac{\partial \mathcal{L}_v}{\partial \boldsymbol{\theta}} \right\| \leq C_v^\theta$ .

According to the implicit function theorem, we have the following lemma.

**Lemma 1 (Implicit Hyperegradient).** Given the GNN model weights  $\boldsymbol{\theta}$  that achieve the local optimum in the inner loop, i.e.,  $\frac{\partial \mathcal{L}}{\partial \boldsymbol{\theta}}|_{\boldsymbol{\theta}=\boldsymbol{\theta}^*} = 0$ , the hypergradient can be equivalently transformed into

$$\nabla_{\boldsymbol{\alpha}} \mathcal{L}_v = \frac{\partial \mathcal{L}_v}{\partial \boldsymbol{\alpha}} - \frac{\partial \mathcal{L}_v}{\partial \boldsymbol{\Theta}} \mathbf{G}_*^{-1} \frac{\partial^2 \mathcal{L}}{\partial \boldsymbol{\alpha} \partial \boldsymbol{\theta}} \Big|_{\boldsymbol{\theta}=\boldsymbol{\theta}^*}, \quad (39)$$

where  $\mathbf{G}_* = \frac{\partial^2 \mathcal{L}}{\partial \boldsymbol{\theta} \partial \boldsymbol{\theta}} \Big|_{\boldsymbol{\theta}=\boldsymbol{\theta}^*}$  denotes the Hessian matrix with respect to  $\boldsymbol{\theta}$  at the point  $\boldsymbol{\theta}^*$ .

*Proof.* From  $\frac{\partial \mathcal{L}}{\partial \boldsymbol{\theta}}|_{\boldsymbol{\theta}=\boldsymbol{\theta}^*} = 0$ , we have

$$\frac{\partial}{\partial \boldsymbol{\alpha}} \left( \frac{\partial \mathcal{L}}{\partial \boldsymbol{\theta}} \Big|_{\boldsymbol{\theta}=\boldsymbol{\theta}^*} \right) = 0. \quad (40)$$

Therefore, we can obtain that

$$\frac{\partial^2 \mathcal{L}}{\partial \boldsymbol{\alpha} \partial \boldsymbol{\theta}} \Big|_{\boldsymbol{\theta}=\boldsymbol{\theta}^*} + \frac{\partial^2 \mathcal{L}}{\partial \boldsymbol{\theta} \partial \boldsymbol{\theta}} \frac{\partial \boldsymbol{\theta}^*(\boldsymbol{\alpha})}{\partial \boldsymbol{\alpha}} \Big|_{\boldsymbol{\theta}=\boldsymbol{\theta}^*} = 0, \quad (41)$$

which can be rearranged as

$$-\frac{\partial^2 \mathcal{L}}{\partial \boldsymbol{\alpha} \partial \boldsymbol{\theta}} \Big|_{\boldsymbol{\theta}=\boldsymbol{\theta}^*} = \frac{\partial^2 \mathcal{L}}{\partial \boldsymbol{\theta} \partial \boldsymbol{\theta}} \Big|_{\boldsymbol{\theta}=\boldsymbol{\theta}^*} \frac{\partial \boldsymbol{\theta}^*(\boldsymbol{\alpha})}{\partial \boldsymbol{\alpha}}. \quad (42)$$

Substituting (42) into (35) yields the implicit hypergradient (39), which completes the proof.  $\square$

However, it is highly computational complexity to calculate the inverse of the Hessian matrix in (39), especially for the GNN with massive neural parameters. Therefore, we introduce the Neumann series expansion to tractably approximate the Hessian matrix inverse, which provides a stable and efficient way for matrix inverse approximation.

**Lemma 2** (Neumann series expansion [28, Theorem 4.20]). The inversion of matrix  $\mathbf{G} \in \mathbb{R}^{N \times N}$  can be transformed into

$$\mathbf{G}^{-1} = \sum_{n=0}^{\infty} (\mathbf{I} - \mathbf{G})^n, \quad (43)$$

if the condition  $\|\mathbf{I} - \mathbf{G}\| < 1$  can be satisfied, with  $\|\cdot\|$  being the spectral norm.

**Lemma 3** (AutoGNN hypergradient). Given a sufficiently small learning rate  $\kappa$  that satisfies  $\kappa < \frac{2}{L^\theta}$ , the implicit hypergradient of the proposed AutoGNN architecture can be transformed based on the Neumann series into

$$\nabla_{\alpha} \mathcal{L}_v = \frac{\partial \mathcal{L}_v}{\partial \alpha} - \kappa \frac{\partial \mathcal{L}_v}{\partial \Theta} \left[ \sum_{n=0}^{\infty} (\mathbf{I} - \kappa \mathbf{G}_*)^n \right] \frac{\partial^2 \mathcal{L}}{\partial \alpha \partial \theta} \Big|_{\theta=\theta^*}. \quad (44)$$

*Proof.* See Appendix A. □

---

**Algorithm 2** Bi-Level AutoGNN Learning Algorithm

---

- 1: Initialize the GNN model weights  $\theta$  and the architecture parameters  $\alpha$ .
  - 2: Set the iteration number as  $t = 0$ .
  - 3: **repeat**
  - 4:   Randomly sample mini-batches of data from the training dataset  $\mathcal{D}_t$ .
  - 5:   Update GNN model weights  $\theta$  based on  $T$ -step gradient descent.
  - 6:   Calculate the Hessian matrix  $\frac{\partial^2 \mathcal{L}^i}{\partial \theta \partial \theta}$ .
  - 7:   Randomly sample mini-batches of data from the validation dataset  $\mathcal{D}_v$ .
  - 8:   Compute the stochastic approximated AutoGNN hypergradient  $\nabla_{\alpha} \hat{\mathcal{L}}_v$  using (46).
  - 9:   Update architecture parameters by  $\alpha \leftarrow \alpha - \kappa \nabla_{\alpha} \hat{\mathcal{L}}_v$ .
  - 10: **until** converge.
- Output:** The optimal GNN architecture parameters  $\alpha$  and model weights  $\theta$ .
- 

By leveraging the first  $N_G$  terms to approximate the Hessian matrix inverse, an approximated version of the implicit hypergradient can be given by

$$\nabla_{\alpha} \tilde{\mathcal{L}}_v = \frac{\partial \mathcal{L}_v}{\partial \alpha} - \kappa \frac{\partial \mathcal{L}_v}{\partial \Theta} \left[ \sum_{n=0}^{N_G} (\mathbf{I} - \kappa \mathbf{G}_*)^n \right] \frac{\partial^2 \mathcal{L}}{\partial \alpha \partial \theta} \Big|_{\theta=\theta^*}. \quad (45)$$

To deal with large-scale datasets in practice, we compute the loss functions based on mini-batches of the training and validation data samples, respectively, denoted as  $\mathcal{L} = \frac{1}{S_t} \sum_{i=1}^{S_t} \mathcal{L}^i$  and  $\mathcal{L}_v = \frac{1}{S_v} \sum_{j=1}^{S_v} \mathcal{L}_v^j$ . Here,  $S_t$  and  $S_v$  are the number of mini-batches sampled from the training and validation datasets, respectively.  $\mathcal{L}^i$  and  $\mathcal{L}_v^j$  are the loss functions respectively computed over the individual mini-batches  $i$  and  $j$ . In this way, we the stochastic approximated AutoGNN hypergradient can be given by

$$\nabla_{\alpha} \hat{\mathcal{L}}_v = \frac{\partial \mathcal{L}_v^j}{\partial \alpha} - \kappa \frac{\partial \mathcal{L}_v^j}{\partial \Theta} \left[ \sum_{n=0}^{N_G} (\mathbf{I} - \kappa \mathbf{G}_*^i)^n \right] \frac{\partial^2 \mathcal{L}^i}{\partial \alpha \partial \theta} \Big|_{\theta=\theta^*}, \quad (46)$$

where  $\mathbf{G}_*^i = \frac{\partial^2 \mathcal{L}^i}{\partial \boldsymbol{\theta} \partial \boldsymbol{\theta}} \big|_{\boldsymbol{\theta}=\boldsymbol{\theta}^*}$ .

Leveraging the stochastic approximated AutoGNN hypergradient, the bi-level AutoGNN learning algorithm can be summarized in Algorithm 2.

### C. Theoretical Analysis

In this subsection, we aim to analyze the performance of the proposed permutation-equivalent property, the approximation error, and the convergence.

Define  $\star \mathcal{M}$  as the permutation operation of the node set  $\mathcal{M}$  and  $\star \mathcal{G}$  ( $\star \mathbf{Z}$ ) as the permutation of graph (optimization variables) corresponding to  $\star \mathcal{M}$ . Furthermore, we define the solution predicted by the GNN as  $\mathbf{Z} = F_A(\star \mathcal{G})$ , where  $F_A$  describes the function of AutoGNN.

**Proposition 1.** The proposed AutoGNN satisfies the permutation equivalence property  $\mathbf{Z} = F_A(\mathcal{G})$ , which satisfies  $F_A(\star \mathcal{G}) = \star(F_A(\mathcal{G})) = \star \mathbf{Z}$ .

*Proof.* By sharing the GNN model weights  $\boldsymbol{\theta}$  and the architecture parameters  $\boldsymbol{\alpha}$  among distributed agents, the proposed auto-learned module would not impact the permutation invariance property, which can be proven referring to [12].  $\square$

The approximation error of the hypergradient is bounded according to the following Lemma.

**Lemma 4.** Based on Assumption 1, the error  $\delta \triangleq \nabla_{\boldsymbol{\alpha}} \mathcal{L}_v - \nabla_{\boldsymbol{\alpha}} \tilde{\mathcal{L}}_v$  between the approximated AutoGNN hypergradient  $\nabla_{\boldsymbol{\alpha}} \tilde{\mathcal{L}}_v$  with  $N_G < \infty$  and the actual hypergradient  $\nabla_{\boldsymbol{\alpha}} \mathcal{L}_v$  with  $N_G \rightarrow \infty$  is upper bounded by

$$\|\delta\| \leq C^{\theta\alpha} C_v^{\theta} \frac{1}{\mu} (1 - \kappa\mu)^{N_G+1}. \quad (47)$$

*Proof.* Considering the definitions of  $\nabla_{\boldsymbol{\alpha}} \tilde{\mathcal{L}}_v$  and  $\nabla_{\boldsymbol{\alpha}} \mathcal{L}_v$ , we have

$$\nabla_{\boldsymbol{\alpha}} \mathcal{L}_v - \nabla_{\boldsymbol{\alpha}} \tilde{\mathcal{L}}_v = \kappa \frac{\partial \mathcal{L}_v}{\partial \boldsymbol{\theta}} \sum_{n=N_G+1}^{\infty} [\mathbf{I} - \kappa \mathbf{G}_*]^n \frac{\partial^2 \mathcal{L}}{\partial \boldsymbol{\alpha} \partial \boldsymbol{\theta}}. \quad (48)$$

Since function  $\mathcal{L}$  is locally  $\mu$ -strongly convex and has Lipschitz-continuous gradient surrounding  $\boldsymbol{\theta}^*$ , we have  $\kappa\mu\mathbf{I} \preceq \kappa\mathbf{G}_* \preceq \mathbf{I}$  with  $\kappa < L^{\theta}$ , which yields

$$\sum_{n=N_G+1}^{\infty} [\mathbf{I} - \kappa \mathbf{G}_*]^n \leq \sum_{n=N_G+1}^{\infty} [1 - \kappa\mu]^n \stackrel{(a)}{\leq} \frac{1}{\kappa\mu} (1 - \kappa\mu)^{N_G+1}, \quad (49)$$

where (a) is obtained using the sum rate of the geometry sequence. Considering  $\left\| \frac{\partial \mathcal{L}_v}{\partial \boldsymbol{\theta}} \right\| \leq C_v^{\theta}$  and  $\left\| \frac{\partial^2 \mathcal{L}}{\partial \boldsymbol{\alpha} \partial \boldsymbol{\theta}} \right\| \leq C^{\theta\alpha}$  and substituting (49) into (48), we have

$$\left\| \nabla_{\boldsymbol{\alpha}} \mathcal{L}_v - \nabla_{\boldsymbol{\alpha}} \tilde{\mathcal{L}}_v \right\| \leq C_v^{\theta} C^{\theta\alpha} \frac{1}{\mu} (1 - \kappa\mu)^{N_G+1}, \quad (50)$$

which ends the proof.  $\square$

Moreover, the convergence performance of the proposed AutoGNN can be characterized by the following theorem.

**Theorem 1.** Under the Assumption 1 - 2, the proposed AutoGNN algorithm using the stochastic approximated hypergradient can converge to a stationary point when the learning rate  $\kappa$  is sufficiently small, namely,

$$\lim_{u \rightarrow \infty} \mathbb{E} \left[ \left\| \nabla_{\alpha} \widehat{\mathcal{L}}_v^i(\Theta^{(u)}, \alpha^{(u)}) \right\| \right] = 0. \quad (51)$$

*Proof.* See Appendix B.  $\square$

## V. SIMULATION RESULTS

In this section, we first introduce several benchmark algorithms based on conventional optimization-based algorithms and conventional fixed GNN. Then, numerical results are presented to verify the effectiveness of the proposed framework and algorithm.

### A. Benchmark Algorithms

1) *Benchmark scheduling methods:* We consider three benchmark algorithms for the joint cluster-free SIC and coordinated beamforming scheduling for multi-cell cluster-free NOMA:

- **Distributed ADMM:** where BSs exchange information during each iteration to achieve distributed optimization without directly sharing CSI. The detailed design is described in Section V-A2.
- **Centralized ADMM:** where BSs directly send their local CSI to a centralized controller, and the multi-cell coordinated beamforming and SIC operations are obtained by solving the MMSE reformulation of  $\mathcal{P}_0$  (see Section V-A2) using the centralized ADMM method.
- **Fixed GNN:** where the GNN employs a conventional fixed architecture, i.e., fixed network depth and fixed message embedding sizes, as described in Section III-B.

2) *Distributed ADMM design:* Distributed ADMM [18] is a general distributed optimization method to deal with non-convex MINLPs, which can achieve locally optimal solutions with few information exchange and low complexity. Here, we develop a benchmark distributed ADMM algorithm for multi-cell cluster-free NOMA scheduling. To deal with the binary variables  $\beta^m$ , we first introduce the auxiliary variable  $\tilde{\beta}^m = \{\tilde{\beta}_{ik}^m\}$  that satisfies

$$\beta^m + \tilde{\beta}^m = \mathbf{1}_{K \times K}, \quad \forall m \in \mathcal{M}, \quad (52)$$

$$\beta_{ik}^m \tilde{\beta}_{ik}^m = 0, \quad \forall i, k \in \mathcal{K}_m, \quad \forall m \in \mathcal{M}, \quad (53)$$

$$0 \leq \beta_{ik}^m \leq 1, \forall i, k \in \mathcal{K}_m, \forall m \in \mathcal{M}. \quad (54)$$

Since constraints (52)-(54) ensure  $\beta_{ik}^m (1 - \beta_{ik}^m) = 0$ , the original binary constraint (6e) can be equivalently replaced. To deal with the max-min problem, we further introduce the slack variable  $\Gamma = \{\Gamma_k^m\}$ , which can be written as  $\Gamma_k^m = \min_{i \in \mathcal{K}_m} \left\{ \frac{1}{\beta_{ik}^m} r_{ik}^m \right\} \leq \frac{1}{\beta_{ik}^m} r_{ik}^m, \forall k \in \mathcal{K}_m, m \in \mathcal{M}$ . Then,  $\mathcal{P}_0$  can be equivalently transferred into

$$\mathcal{P}_1 : \max_{\Gamma, \beta, \tilde{\beta}, \mathbf{W}} \sum_{m \in \mathcal{M}} \sum_{k \in \mathcal{K}_m} \Gamma_k^m \quad (55a)$$

$$\text{s.t. } \beta_{ik}^m \Gamma_k^m \leq r_{ik}^m, \forall k \in \mathcal{K}_m, \forall m \in \mathcal{M}, \quad (55b)$$

$$\Gamma_k^m \geq r_k^{m, \min}, \forall k \in \mathcal{K}_m, \forall m \in \mathcal{M}, \quad (55c)$$

$$(6c) - (6d), (52) - (54). \quad (55d)$$

To solve  $\mathcal{P}_1$ , we employ the MMSE [29] to handle the non-convex data rate expression. Based on the MMSE detection, the decoding rate can be written as

$$r_{ik}^m = \max_{c_{ik}^m} \max_{a_{ik}^m > 0} \left( \log_2 a_{ik}^m - \frac{a_{ik}^m \epsilon_{ik}^m}{\ln 2} + \frac{1}{\ln 2} \right), \forall i, k \in \mathcal{K}_m, m \in \mathcal{M}, \quad (56)$$

where  $\epsilon_{ik}^m$  denotes the mean square error (MSE), which can be given by

$$\epsilon_{ik}^m = 1 - 2\text{Re}(c_{ik}^m \mathbf{h}_{mi}^m \mathbf{w}_u^m) + |c_{ik}^m|^2 (|\mathbf{h}_{mi}^m \mathbf{w}_k^m|^2 + \text{Intf}_{ik}^m + \sigma^2), \forall i, k \in \mathcal{K}_m, m \in \mathcal{M}, \quad (57)$$

and  $c_{ik}^m$  indicates the channel equalization coefficient. From (56), the lower bound of  $r_{ik}^m$  can be formulated as  $r_{ik}^m \geq \log_2 a_{ik}^m - \frac{a_{ik}^m \epsilon_{ik}^m}{\ln 2} + \frac{1}{\ln 2}$ . Hence, constraint (55b) can be rewritten as

$$\beta_{ik}^m \Gamma_k^m \leq \log_2 a_{ik}^m - \frac{a_{ik}^m \epsilon_{ik}^m}{\ln 2} + \frac{1}{\ln 2}, \forall i, k \in \mathcal{K}_m, m \in \mathcal{M}. \quad (58)$$

On the other hand, to deal with the high coupling variables  $\beta_{iu}^m, \beta_{uk}^m$ , and  $\beta_{ku}^m$  in  $\text{Intf}_{ik}^m(\tilde{\beta}^m, \mathbf{W})$ , we rearrange (2) as

$$\begin{aligned} \text{Intf}_{ik}^m(\tilde{\beta}^m, \mathbf{W}) &= \underbrace{\sum_{u < k} \max\{\tilde{\beta}_{iu}^m, 1 - \tilde{\beta}_{uk}^m\} |\mathbf{h}_{mi}^m \mathbf{w}_u^m|^2}_{\text{intra-cell interference from weaker users}} + \underbrace{\sum_{u > k} \max\{\tilde{\beta}_{iu}^m, \tilde{\beta}_{ku}^m\} |\mathbf{h}_{mi}^m \mathbf{w}_u^m|^2}_{\text{intra-cell interference from stronger users}} \\ &\quad + \text{ICI}_i^m(\mathbf{W}), \forall i \neq k, i, k \in \mathcal{K}_m, m \in \mathcal{M}. \end{aligned} \quad (59)$$

Since  $\max\{f(x), g(x)\}$  is convex when both functions  $f(x)$  and  $g(x)$  are convex,  $\text{Intf}_{ik}^m(\tilde{\beta}^m, \mathbf{W})$  in (59) is convex over  $\tilde{\beta}$ . Thereafter, problem  $\mathcal{P}_1$  can be transferred into a multi-convex problem over  $\{c_{ik}^m\}, \{a_{ik}^m\}, \Gamma, \beta, \tilde{\beta}$ , and  $\mathbf{W}$ . However, this multi-convex problem still cannot be directly decomposed among the distributed BSs owing to the ICI terms. To decouple ICI, we introduce a slack variable  $\xi_{mnk}$  that indicates the upper bound of ICI from BS  $m$  to user  $k$  served by BS  $n$ . Let  $\hat{\xi}_{mnk}^m$  denote the global copy of  $\xi_{mnk}$ . Moreover, each BS  $m$  locally store the local copies

$\xi_{mnk}^m$  and  $\xi_{nmk}^m$ , which correspond to the ICI terms  $\xi_{mnk}$  and  $\xi_{nmk}$  related to BS  $m$ , respectively. At each BS  $m$ , the local variable  $\xi_{mnk}^{m,(t)}$  satisfies

$$\xi_{mnk}^m \geq \sum_{u \in \mathcal{K}_m} |\mathbf{h}_{nk}^m \mathbf{w}_u^m|^2, \quad \forall n \neq m, \quad k \in \mathcal{K}_n, \quad m \in \mathcal{M}. \quad (60)$$

Let  $\boldsymbol{\xi}^m = [\xi_{m11}^m, \xi_{m12}^m, \dots, \xi_{m1K}^m, \dots, \xi_{mMK}^m, \xi_{1m1}^m, \xi_{1m2}^m, \dots, \xi_{1mK}^m, \dots, \xi_{MmK}^m]$  stack all local copies of ICI variables stored at BS  $m$ . Then, the consensus between distributed BSs can be achieved by forcing the the local copy  $\boldsymbol{\xi}^m$  and the global copy  $\hat{\boldsymbol{\xi}}^m$  to be equal, i.e.,

$$\hat{\boldsymbol{\xi}}^m = \boldsymbol{\xi}^m, \quad \forall m \in \mathcal{M}. \quad (61)$$

Therefore, we can equivalently transform  $\mathcal{P}_1$  as

$$\mathcal{P}_2 : \max_{\boldsymbol{\Gamma}, \mathbf{W}, \boldsymbol{\beta}, \tilde{\boldsymbol{\beta}}, \boldsymbol{\xi}, \hat{\boldsymbol{\xi}}} \sum_{m \in \mathcal{M}} \sum_{k \in \mathcal{K}_m} \Gamma_k^m \quad (62a)$$

$$\text{s.t. } \beta_{ik}^m(t) \Gamma_k^m \leq \log_2 a_{ik}^m - \frac{a_{ik}^m \tilde{\epsilon}_{ik}^m}{\ln 2} + \frac{1}{\ln 2}, \quad \forall i, k \in \mathcal{M}_k, m \in \mathcal{M}, \quad (62b)$$

$$(6c) - (6d), (52) - (54), (55c), (60) - (61). \quad (62c)$$

Here,  $\tilde{\epsilon}_{ik}^m$  indicates the local copy of  $\epsilon_{ik}^m$  that replaces  $\text{ICI}_{ik}^m$  in (57) as  $\widetilde{\text{ICI}}_i^m = \sum_{n \neq m} \xi_{nmi}^m$ . Based on the ADMM framework, the augmented Lagrangian of  $\mathcal{P}_2$  can be formulated as

$$\begin{aligned} \mathcal{L}_A(\boldsymbol{\omega}^{(t)}, \hat{\boldsymbol{\xi}}; \boldsymbol{\lambda}, \tilde{\boldsymbol{\lambda}}, \boldsymbol{\nu}) &= \sum_m \mathcal{L}_A^m(\boldsymbol{\omega}^m, \hat{\boldsymbol{\xi}}^m; \boldsymbol{\lambda}^m, \tilde{\boldsymbol{\lambda}}^m, \boldsymbol{\nu}^m) = \sum_m \left[ \sum_{k \in \mathcal{K}_m} \Gamma_k^{m,(t)} - \right. \\ &\left. \frac{1}{2\rho} \left\| \boldsymbol{\beta}^m + \tilde{\boldsymbol{\beta}}^m - \mathbf{1}_{K \times K} + \rho \boldsymbol{\lambda}^m \right\|^2 - \frac{1}{2\rho} \sum_{i,k \in \mathcal{M}_k} \left( \beta_{ik}^m \tilde{\beta}_{ik}^m + \rho \tilde{\lambda}_{ik}^m \right)^2 - \frac{1}{2\rho} \left\| \boldsymbol{\xi}^m - \hat{\boldsymbol{\xi}}^m + \rho \boldsymbol{\nu}^{m,(t)} \right\|^2 \right], \end{aligned}$$

where  $\boldsymbol{\lambda}$ ,  $\tilde{\boldsymbol{\lambda}}$ , and  $\boldsymbol{\nu}$  represent the dual variables corresponding to equality constraints (52), (53), and (60), respectively.  $\boldsymbol{\omega}^m = \{\boldsymbol{\Gamma}^m, \mathbf{W}^m, \boldsymbol{\beta}^m, \tilde{\boldsymbol{\beta}}^m, \boldsymbol{\xi}^m, \tilde{\boldsymbol{\alpha}}^m, \tilde{\boldsymbol{c}}^m\}$  stacks the variables that can be locally solved at each BS  $m$ . During each iteration  $t$ , the distributed ADMM alternately updates the global variables  $\hat{\boldsymbol{\xi}}$ , local variables  $\boldsymbol{\omega}$ , and dual variables  $\{\boldsymbol{\lambda}, \tilde{\boldsymbol{\lambda}}, \boldsymbol{\nu}\}$  as follows.

**(i) Global variable update.** At each iteration  $t$ , global variables  $\hat{\boldsymbol{\xi}}_{mn}^{(t)} = [\hat{\xi}_{mn1}^{(t)}, \hat{\xi}_{mn2}^{(t)}, \dots, \hat{\xi}_{mnK}^{(t)}]$  can be updated by solving  $\hat{\boldsymbol{\xi}}_{mn}^{(t)} = \arg \min_{\hat{\boldsymbol{\xi}}_{mn}^{(t)}} \frac{1}{2\rho} (\boldsymbol{\xi}_{mn}^{m,(t-1)} - \hat{\boldsymbol{\xi}}_{mn}^{(t)} + \rho \boldsymbol{\nu}_{mn}^{m,(t-1)})^2 + \frac{1}{2\rho} (\boldsymbol{\xi}_{mn}^{n,(t-1)} - \hat{\boldsymbol{\xi}}_{mn}^{(t)} + \rho \boldsymbol{\nu}_{mn}^{n,(t-1)})^2$ . The solution to this unconstrained convex quadratic programming can be derived as

$$\hat{\boldsymbol{\xi}}_{mn}^{(t)} = \frac{1}{2} [\boldsymbol{\xi}_{mn}^{m,(t-1)} + \boldsymbol{\xi}_{mn}^{n,(t-1)} + \rho (\boldsymbol{\nu}_{mn}^{m,(t-1)} + \boldsymbol{\nu}_{mn}^{n,(t-1)})]. \quad (63)$$

From (63), we can observe that only the information of  $[\boldsymbol{\xi}_{mn}^{m,(t-1)} + \frac{1}{\rho} \boldsymbol{\nu}_{mn}^{m,(t-1)}, \boldsymbol{\xi}_{nm}^{m,(t-1)} + \frac{1}{\rho} \boldsymbol{\nu}_{nm}^{m,(t-1)}]$  and  $[\boldsymbol{\xi}_{mn}^{n,(t-1)} + \frac{1}{\rho} \boldsymbol{\nu}_{mn}^{n,(t-1)}, \boldsymbol{\xi}_{nm}^{n,(t-1)} + \frac{1}{\rho} \boldsymbol{\nu}_{nm}^{n,(t-1)}]$  should be exchanged between BS  $m$  and BS  $n$  to update  $\hat{\boldsymbol{\xi}}_{mn}^{(t)}$  and  $\hat{\boldsymbol{\xi}}_{nm}^{(t)}$  during each iteration.

(ii) **Local variable update.** Given  $\hat{\xi}^{m,(t)}$  and dual variables  $\{\lambda^{m,(t-1)}, \tilde{\lambda}^{m,(t-1)}, \nu^{m,(t-1)}\}$ , each BS  $m$  locally solve the decomposed variables  $\omega^{m,(t)}$  in a distributed and parallel way. Based on alternative optimization,  $\tilde{a}_{ik}^{m,(t)}$  and  $\tilde{c}_{ik}^{m,(t)}$  can be respectively updated by

$$\tilde{a}_{ik}^{m,(t)} = \left( \left| \mathbf{h}_{mi}^m \mathbf{w}_k^{m,(t-1)} \right|^2 + \widetilde{\text{Intf}}_{ik}^{m,(t-1)} + \sigma^2 \right) \left( \widetilde{\text{Intf}}_{ik}^{m,(t-1)} + \sigma^2 \right)^{-1}, \quad (64)$$

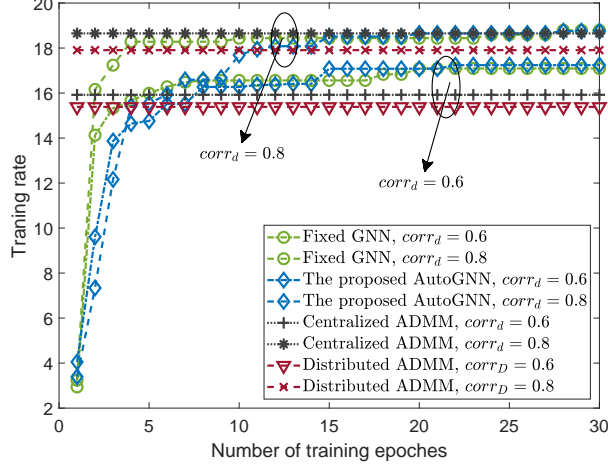
$$\tilde{c}_{ik}^{m,(t)} = \left( \mathbf{h}_{mi}^m \mathbf{w}_k^{m,(t-1)} \right)^H \left( \left| \mathbf{h}_{mi}^m \mathbf{w}_k^{m,(t-1)} \right|^2 + \widetilde{\text{Intf}}_{ik}^{m,(t-1)} + \sigma^2 \right)^{-1}. \quad (65)$$

Define  $\omega^m \in \Omega^m = \{\omega^m | (6c) - (6d), (54), (60), (62b)\}, \forall m \in \mathcal{M}$  as the local feasible set of  $\omega_m$ . Thereafter, variables  $\xi^m, \beta^m, \tilde{\beta}^m, \mathbf{W}^m$ , and  $\Gamma^m$  can be alternatively updated by solving the convex subproblems  $\{\xi^m, \beta^m\} = \arg \min_{\xi^m, \beta^m \in \Omega^m} \mathcal{L}_A^m(\omega^m, \hat{\xi}^m; \lambda^m, \tilde{\lambda}^m, \nu^m)$  and  $\{\Gamma^m, \mathbf{W}^m, \tilde{\beta}^m\} = \arg \min_{\Gamma^m, \mathbf{W}^m, \tilde{\beta}^m \in \Omega^m} \mathcal{L}_A^m(\omega^m, \hat{\xi}^m; \lambda^m, \tilde{\lambda}^m, \nu^m)$ . Moreover, the dual variables can be updated by  $\lambda^{m,(t+1)} = \lambda^{m,(t)} + \frac{1}{\rho}(\beta^{m,(t)} + \tilde{\beta}^{m,(t)} - \mathbf{1}_{K \times K})$ ,  $\tilde{\lambda}_{ik}^{m,(t+1)} = \tilde{\lambda}_{ik}^{m,(t)} + \frac{1}{\rho} \tilde{\beta}_{ik}^{m,(t)} \beta_{ik}^{m,(t)}$ , and  $\nu^{m,(t+1)} = \nu^{m,(t)} + \frac{1}{\rho}(\xi^{m,(t)} - \hat{\xi}^{m,(t)})$ .

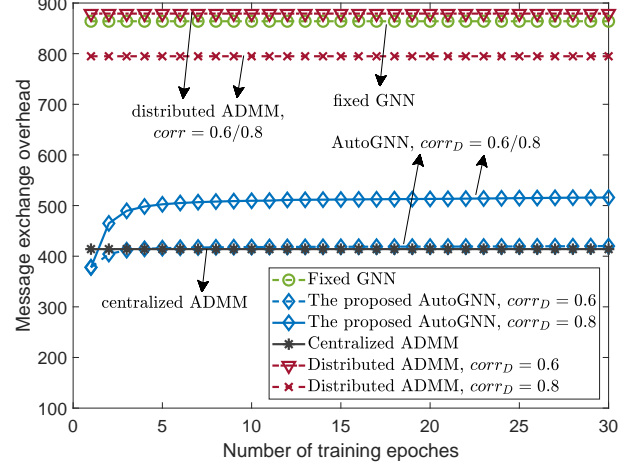
## B. Numerical Results

We consider  $M = 3$  coordinated BSs, where each BS equips  $N_T = 4$  antennas. The maximum transmit power at each BS is  $P^{\max} = 27$  dBm, and the signal-to-noise-ratio (SNR) is 20 dB. We assume the number of users served by each BS is  $K = 6$ , and users' minimum rate requirements are  $R_k^{\min} = 0.4$  bps/Hz,  $\forall k$ . We further model the data channel  $\mathbf{H}_{mm}$  and the interference channel  $\mathbf{H}_{mn}, \forall m \neq n$ , according to [30], where the mean correlations of data channels and interference channels are set as  $\text{corr}_D = \{0.5, 0.55, 0.6, 0.65, 0.7, 0.75, 0.8\}$  and  $\text{corr}_I = 0.5$ , respectively. For the conventional fixed GNN, the layer number is set as  $L = 4$ , and the embedding size is 36. We randomly generate 100 mini-batches for the training dataset, 50 mini-batches for the validation dataset, and 10 mini-batches for the test dataset, where each mini-batch consists of 64 data samples. Since both the centralized/distributed ADMM algorithms have high computation complexity, it is impractical to label the large-scale training dataset. Hence, we train both the fixed GNN and the AutoGNN in an unsupervised-learning manner.

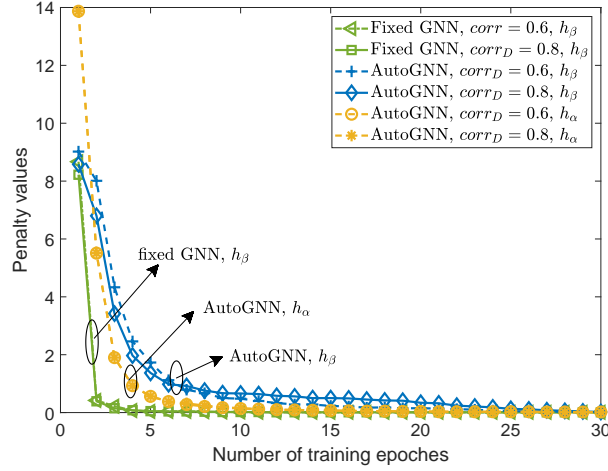
In Fig. 3, we compare the convergence behaviors for training the AutoGNN and the conventional fixed GNN. To confirm the effectiveness, we also present the performances of two optimization-based benchmarks, namely the distributed ADMM and the centralized ADMM algorithms. For the centralized/distributed ADMM algorithm, we select the initialized parameters by testing 20 different initializations. Fig. 3(a) shows both the fixed GNN and the AutoGNN achieve comparable system sum rate with the centralized ADMM algorithm and outperform the



(a) Sum rate versus number of training epochs.



(b) Exchanged message size versus number of training epochs.



(c) Penalty values versus number of training epochs.

Fig. 3: Convergence comparisons among the proposed algorithm and the benchmarks.

distributed ADMM algorithm, which validates that the learning-based algorithms can effectively overcome the parameter initialization dependance issue and achieve efficient coordination. In Fig. 3(b), the resulting message overheads of the AutoGNN increase with the number of epochs, and converges eventually. The centralized ADMM yields the least message exchange overhead and outperforms distributed ADMM, since it directly collects the information from BSs and computes in a centralized controller. Moreover, the distributed ADMM leads to the highest message exchange overhead, since it relies on information exchange during each iteration and requires a large number of iterations for realize distributed scheduling. Compared with the fixed GNN, AutoGNN can significantly reduce the message exchange overhead without degrading the system performance. In Fig. 3(c), the penalty terms  $h_\beta$  and  $h_\alpha$  decrease with the number



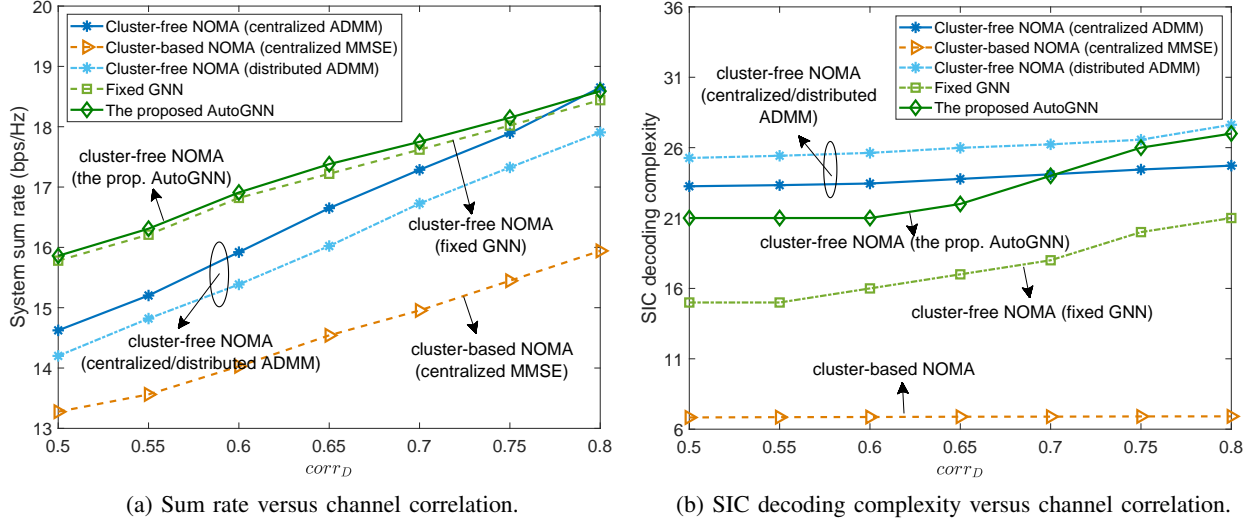


Fig. 4: System performance comparisons under different data channel correlations.

of epoches, and eventually vanish to zeros within 30 epoches, which signifies that the integer constraints of both SIC operations and the architecture parameters can be satisfied. Since the AutoGNN needs to jointly train the GNN weight parameters and the architecture parameters, its convergence speed is relatively slower than the fixed GNN.

Fig. 4 presents the system performance comparisons among different algorithms under various data channel correlations. Besides the proposed benchmarks, we also introduce the conventional cluster-based NOMA mechanism to illustrate the performance gains of the proposed cluster-free NOMA scheme. Specifically, the cluster-based NOMA mechanism performs the user clustering based on the channel correlations [29], and the beamforming vectors of users are optimized in a centralized way based on the MMSE reformulation. Here, the results of all algorithms are averaged over the test dataset.

In Fig. 4(a), the proposed multi-cell cluster-free NOMA framework outperforms cluster-based NOMA under different data channel correlations. Moreover, the rate performance gap increases with the data channel correlations. The learning-based GNN algorithms outperform conventional distributed ADMM algorithms, which demonstrates that the GNN algorithm results an efficient interaction mechanism to facilitate multi-agent coordination. Moreover, the proposed AutoGNN yields higher system sum rate than conventional fixed GNN, and achieves comparable performance with the well-tuned centralized ADMM algorithm, since it can learn an optimized architecture. On the other hand, Fig. 4(b) compares the SIC decoding complexity, i.e.,  $\sum_{m \in \mathcal{M}} \sum_{i \in \mathcal{K}} \sum_{k \in \mathcal{K}, i \neq k} \beta_{ik}^m$ , between different algorithms. The proposed framework enables

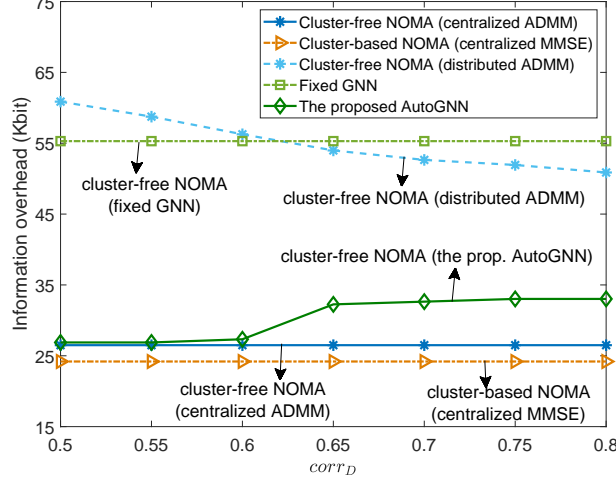


Fig. 5: Information overheads among the proposed algorithm and the benchmarks.

TABLE I: Comparisons of Computation/Communication Overheads for Different Algorithms,  $corr_D = 0.6$

Method	Test sum rate (bps/Hz)	Execution time	Number of GNN layers/iterations	Information overhead (Kbit)
Centralized ADMM	15.92	12.41 min/sample	23.78	<b>26.49</b>
Distributed ADMM	15.38	5.86 min/sample	25.54	56.26
Fixed GNN	16.82	2.82 ms/batch	4	55.29
AutoGNN	<b>16.91</b>	<b>2.69 ms/batch</b>	<b>3</b>	26.88

higher SIC decoding complexity than conventional cluster-based NOMA, and the SIC decoding complexity adaptively increases with users' data channel correlations. It is verified that the proposed framework has a higher flexibility to deal with different scenarios. Moreover, the SIC decoding complexity of the AutoGNN can approach the centralized ADMM algorithm better than the fixed GNN.

Fig. 5 shows the information overheads among different algorithms under different data channel correlations  $corr_D$ . Here, each floating point number in the exchanged information takes up 64 bit. In Fig. 5, the distributed ADMM algorithm suffers high information overheads due to the slow convergence. Moreover, the communication overheads of the proposed AutoGNN increase with data channel correlations, which may be due to that higher data channel correlations lead to higher SIC decoding complexity and require more sophisticated distributed control. Compared with the conventional distributed ADMM and the fixed GNN, the proposed AutoGNN can significantly and adaptively reduce the information overheads under different data channel correlations, which demonstrates the effectiveness of the auto-learning architecture.

Detailed results are presented in Table I to compare the computation and communication overheads among these algorithms. Here, we set  $corr_D = 0.6$ . The centralized ADMM achieves the least information overheads at the cost of the longest execution time, whilst the fixed GNN

can overcome the slow convergence of conventional optimization-based methods at the cost of high communication overheads. In contrast, the AutoGNN can achieve the fastest time response and significantly reduce the information overhead, which is capable of learning a computation- and communication-efficient architecture for intelligent distributed scheduling.

## VI. CONCLUSION

A novel multi-cell cluster-free NOMA framework has been proposed in this paper, where the coordinated beamforming and cluster-free SIC were jointly designed to efficiently suppress both intra-cell and inter-cell interference. The objective function is formulated to maximize the system sum rate while ensuring the SIC decoding requirements and users' data rate constraints. To deal with this highly complex and coupling MINLP problem, a novel communication-efficient distributed AutoGNN architecture was proposed, which can automatically learn the suitable GNN architecture to reduce computation and information exchange burdens. To jointly train the GNN weights and architecture parameters for distributed beamforming and SIC optimization, a bi-level AutoGNN learning algorithm was further developed, which was theoretically proven to converge to a stationary point. Our numerical results demonstrated that the cluster-free NOMA outperforms conventional cluster-based NOMA under multi-cell scenarios. Moreover, compared with the conventional fixed GNN and distributed ADMM algorithms, the proposed AutoGNN can adaptively reduce the information exchange overheads without degrading the system performance, which verified the effectiveness of the proposed algorithm.

## APPENDIX

### A. Proof of Lemma 3

Let  $v(\mathbf{G}_*)$  collect all the eigenvalues of the Hessian matrix  $\mathbf{G}_*$ . Using condition (iii) in Assumption 1, the eigenvalues  $v(\mathbf{G}_*)$  are lower bounded by  $0 < \mu \leq v(\mathbf{G}_*)$ . Using condition (ii) in Assumption 1, the eigenvalues  $v(\mathbf{G}_*)$  are upper bounded by  $\tilde{L}^\theta$ , namely,  $\mathbf{G}_* \preceq \tilde{L}^\theta \mathbf{I} \Rightarrow 0 < v(\mathbf{G}_*) \leq \tilde{L}^\theta$ . Since  $v(\kappa \mathbf{G}_*) = \kappa[v(\mathbf{G}_*)]$ , given a learning rate  $\kappa < \frac{2}{\tilde{L}^\theta}$ , we have  $0 < \kappa[v(\mathbf{G}_*)] < \kappa \tilde{L}^\theta < 2$ . Hence, we can achieve that

$$-1 < v(\kappa \mathbf{G}_* - \mathbf{I}) = \nu(\kappa \mathbf{G}_*) - 1 < 1. \quad (66)$$

Since the spectral norm  $\|\kappa \mathbf{G}_* - \mathbf{I}\| = \|\mathbf{I} - \kappa \mathbf{G}_*\| = \max\{|v(\kappa \mathbf{G}_* - \mathbf{I})|\}$ , from (66) we can obtain  $\|\mathbf{I} - \kappa \mathbf{G}_*\| < 1$ . According to Lemma 2,  $\mathbf{G}_*^{-1}$  can be approximated by the Neumann series expansion (43) as

$$\mathbf{G}_*^{-1} = \kappa (\kappa \mathbf{G}_*)^{-1} = \kappa \sum_{n=0}^{\infty} (\mathbf{I} - \kappa \mathbf{G}_*)^n. \quad (67)$$

Substituting (67) into (39), the implicit hypergradient defined in (39) can be rewritten as (44), which ends the proof.

### B. Proof of Theorem 1

Let  $\nabla_{\alpha} \mathcal{L}_v^{(u)} \triangleq \nabla_{\alpha} \mathcal{L}_v (\Theta^{(u)}, \alpha^{(u)})$  and  $\nabla_{\alpha} \mathcal{L}_v^{i,(u)} \triangleq \mathcal{L}_v^i (\Theta^{(u)}, \alpha^{(u)})$  denote the exact hypergradient and the non-approximated stochastic hypergradient with  $N_G \rightarrow \infty$  at each outer-loop iteration  $u$ , respectively. Define  $\varepsilon^{(u)} \triangleq \nabla_{\alpha} \mathcal{L}_v^{(u)} - \nabla_{\alpha} \mathcal{L}_v^{i,(u)}$  as the noise between the exact hypergradient and the stochastic hypergradient. Considering the derived implicit hypergradient (39), by taking the expectation over all mini-batches we have

$$\mathbb{E} [\nabla_{\alpha} \mathcal{L}_v^{i,(u)}] = \mathbb{E} \left[ \frac{\partial^2 \mathcal{L}_v^{i,(u)}}{\partial \alpha} - \frac{\partial \mathcal{L}_v^{i,(u)}}{\partial \theta} \left( \frac{\partial^2 \mathcal{L}^j (\theta, \alpha^{(u)})}{\partial \theta \partial \theta} \right)^{-1} \frac{\partial \mathcal{L}^j (\theta, \alpha^{(u)})}{\partial \alpha \partial \theta} \right]. \quad (68)$$

According to [22], the stochastic gradient  $\nabla_{\alpha} \mathcal{L}_v^i$  provides an unbiased estimate of  $\nabla_{\alpha} \mathcal{L}_v$ , i.e.,  $\mathbb{E} [\varepsilon^{(u)}] \triangleq \mathbb{E} [\nabla_{\alpha} \mathcal{L}_v^{i,(u)} - \nabla_{\alpha} \mathcal{L}_v^{(u)}] = 0$ .

On the other hand, since function  $\nabla_{\alpha} \mathcal{L}_v^{(u)}$  is Lipschitz continuous with constant  $\tilde{L}_v^{\alpha}$ , the following inequality holds according to the Lipschitz condition:

$$\begin{aligned} \mathbb{E} [\mathcal{L}_v^{(u+1)}] &\leq \mathbb{E} [\mathcal{L}_v^{(u)}] + \mathbb{E} [\langle \nabla_{\alpha} \mathcal{L}_v^{(u)}, \alpha^{(u+1)} - \alpha^{(u)} \rangle] + \frac{\tilde{L}_v^{\alpha}}{2} \mathbb{E} [\|\alpha^{(u+1)} - \alpha^{(u)}\|^2] \\ &= \mathbb{E} [\mathcal{L}_v^{(u)}] + \left\langle \mathbb{E} [\nabla_{\alpha} \mathcal{L}_v^{(u)}], -\kappa^{(u)} \mathbb{E} [\nabla_{\alpha} \mathcal{L}_v^{i',(u)}] \right\rangle + \frac{\tilde{L}_v^{\alpha}}{2} (\kappa^{(u)})^2 \mathbb{E} [\|\nabla_{\alpha} \mathcal{L}_v^{i',(u)}\|^2]. \end{aligned} \quad (69)$$

For the sake of notation, we further denote  $\nabla_{\alpha} \tilde{\mathcal{L}}_v^{(u)} = \nabla_{\alpha} \tilde{\mathcal{L}}_v (\Theta^{(u)}, \alpha^{(u)})$ . From the definitions we have the following relationships:

$$\mathbb{E} [\nabla_{\alpha} \mathcal{L}_v^{i',(u)}] = \mathbb{E} [\nabla_{\alpha} \mathcal{L}_v^{(u)}] + \mathbb{E} [\varepsilon^{(u)}] \stackrel{\mathbb{E}[\varepsilon^{(u)}]=0}{=} \mathbb{E} [\nabla_{\alpha} \tilde{\mathcal{L}}_v^{(u)}] + \mathbb{E} [\delta^{(u)}], \quad (70)$$

$$\mathbb{E} [\|\nabla_{\alpha} \mathcal{L}_v^{i',(u)}\|^2] = \mathbb{E} [\|\nabla_{\alpha} \mathcal{L}_v^{(u)} + \varepsilon^{(u)}\|^2] \stackrel{\mathbb{E}[\varepsilon^{(u)}]=0}{=} \mathbb{E} [\|\nabla_{\alpha} \mathcal{L}_v^{(u)}\|^2] + \mathbb{E} [\|\varepsilon^{(u)}\|^2], \quad (71)$$

based on which we can rearrange (69) as

$$\begin{aligned} \mathbb{E} [\mathcal{L}_v^{(u+1)}] &\leq \mathbb{E} [\mathcal{L}_v^{(u)}] - \kappa^{(u)} \mathbb{E} [\|\nabla_{\alpha} \tilde{\mathcal{L}}_v^{(u)}\|^2] - \kappa^{(u)} \mathbb{E} [\langle \delta^{(u)}, \nabla_{\alpha} \tilde{\mathcal{L}}_v^{(u)} \rangle] \\ &\quad + \frac{\tilde{L}_v^{\alpha}}{2} (\kappa^{(u)})^2 \mathbb{E} [\|\nabla_{\alpha} \tilde{\mathcal{L}}_v^{(u)}\|^2] + \frac{\tilde{L}_v^{\alpha}}{2} (\kappa^{(u)})^2 \mathbb{E} [\|\varepsilon^{(u)}\|^2]. \end{aligned} \quad (72)$$

Due to  $\|\delta^{(u)}\| \leq C_v^{\theta} C^{\theta \alpha} \frac{1}{\mu} (1 - \kappa \mu)^{N_G + 1}$  from **Lemma 4**, we have  $\langle \delta^{(u)}, \nabla_{\alpha} \tilde{\mathcal{L}}_v^{(u)} \rangle \geq -\Omega \|\nabla_{\alpha} \tilde{\mathcal{L}}_v^{(u)}\|^2$ , where  $\Omega \triangleq \frac{C_v^{\theta} C^{\theta \alpha} (1 - \kappa \mu)^{N_G + 1}}{\mu \|\nabla_{\alpha} \tilde{\mathcal{L}}_v^{(u)}\|}$ . Generally, in the stochastic bi-level gradient learning algorithm we can assume that  $\mathbb{E} [\|\varepsilon^{(u)}\|^2] \leq \Gamma \|\nabla_{\alpha} \tilde{\mathcal{L}}_v^{(u)}\|^2$  [22], [25]. Hence, (72) can be recast as

$$\mathbb{E} [\mathcal{L}_v^{(u+1)}] \leq \mathbb{E} [\mathcal{L}_v^{(u)}] - \kappa^{(u)} \left[ 1 - \Omega - \frac{\tilde{L}_v^\alpha}{2} \kappa^{(u)} (1 + \Gamma) \right] \mathbb{E} \left[ \left\| \nabla_{\alpha} \tilde{\mathcal{L}}_v^{(u)} \right\|^2 \right]. \quad (73)$$

Hence, by choosing appropriate  $N_G$  and a small enough learning rate  $\kappa$  with  $0 < 1 - \kappa\mu < 1$  we can guarantee that  $\Omega < 1$ . Moreover, by ensuring  $\kappa^{(u)} < \frac{2(1-\Omega)}{\tilde{L}_v^\alpha(1+\Gamma)}$ , we have  $1 - \Omega - \frac{\tilde{L}_v^\alpha}{2} \kappa^{(u)} (1 + \Gamma) > 0$ , which means that

$$\mathbb{E} [\mathcal{L}_v^{(u+1)}] \leq \mathbb{E} [\mathcal{L}_v^{(u)}]. \quad (74)$$

Since  $\mathcal{L}_v$  is bounded due to the limited transmit power and the mutual interference,  $\mathcal{L}_v$  can be decreased by the outer loop update until reach convergence. Additionally, we have

$$\mathbb{E} [\mathcal{L}_v^{(u)}] - \mathbb{E} [\mathcal{L}_v^{(u+1)}] \geq \kappa^{(u)} \left[ 1 - \Omega - \frac{\tilde{L}_v^\alpha}{2} \kappa^{(u)} (1 + \Gamma) \right] \mathbb{E} \left[ \left\| \nabla_{\alpha} \tilde{\mathcal{L}}_v^{(u)} \right\|^2 \right]. \quad (75)$$

By summing over  $u = 0, 1, \dots, T_{\text{out}}$ , we have

$$\mathbb{E} [\mathcal{L}_v^{(0)}] - \mathbb{E} [\mathcal{L}_v^{T_{\text{out}}}] \geq \sum_{u=0}^{T_{\text{out}}} \kappa^{(u)} \left[ 1 - \Omega - \frac{\tilde{L}_v^\alpha}{2} \kappa^{(u)} (1 + \Gamma) \right] \mathbb{E} \left[ \left\| \nabla_{\alpha} \tilde{\mathcal{L}}_v^{(u)} \right\|^2 \right]. \quad (76)$$

Since  $\mathcal{L}_v$  has the lower bound, we have  $\lim_{T_{\text{out}} \rightarrow \infty} \sum_{u=0}^{T_{\text{out}}} \kappa^{(u)} \left[ 1 - \Omega - \frac{\tilde{L}_v^\alpha}{2} \kappa^{(u)} (1 + \Gamma) \right] \mathbb{E} \left[ \left\| \nabla_{\alpha} \tilde{\mathcal{L}}_v^{(u)} \right\|^2 \right] < \infty$ . When the learning rate  $\kappa^{(u)}$  in each outer-loop iteration  $u$  satisfies  $\sum_{u=1}^{\infty} \kappa^{(u)} = \infty$  and  $\sum_{u=1}^{\infty} (\kappa^{(u)})^2 < \infty$  [31], we have  $\lim_{T_{\text{out}} \rightarrow \infty} \sum_{n=0}^{T_{\text{out}}} \kappa^{(u)} \left[ 1 - \Omega - \frac{\tilde{L}_v^\alpha}{2} \kappa^{(u)} (1 + \Gamma) \right] = \infty$ , which indicates that  $\lim_{u \rightarrow \infty} \mathbb{E} \left[ \left\| \nabla_{\alpha} \tilde{\mathcal{L}}_v^{(u)} \right\|^2 \right] = 0$ . This completes the proof.

## REFERENCES

- [1] W. Saad, M. Bennis and M. Chen, "A vision of 6G wireless systems: applications, trends, technologies, and open research problems," *IEEE Netw.*, vol. 34, no. 3, pp. 134-142, May/Jun. 2020.
- [2] X. Chen, D. W. K. Ng, W. Yu, E. G. Larsson, N. Al-Dhahir and R. Schober, "Massive access for 5G and beyond," *IEEE J. Sel. Areas Commun.*, vol. 39, no. 3, pp. 615-637, Mar. 2021.
- [3] Y. Liu, S. Zhang, X. Mu, Z. Ding, R. Schober, N. Al-Dhahir, E. Hossain, and X. Shen, "Evolution of NOMA toward next generation multiple access (NGMA) for 6G," *IEEE J. Sel. Areas Commun.*, early access, 2022.
- [4] X. Xu, Y. Liu, X. Mu, Q. Chen, Z. Ding, "A generalized cluster-free NOMA framework towards next-generation multiple access," 2022, *arXiv:2203.15152*. [Online]. Available: <http://arxiv.org/abs/2203.15152>
- [5] Z. Ding, F. Adachi and H. V. Poor, "The application of MIMO to non-orthogonal multiple access," *IEEE Trans. Wireless Commun.*, vol. 15, no. 1, pp. 537-552, Jan. 2016.
- [6] Z. Ding, Y. Liu, J. Choi, Q. Sun, M. Elkashlan, I. Chih-Lin, and H. V. Poor, "Application of non-orthogonal multiple access in LTE and 5G networks," *IEEE Commun. Mag.*, vol. 55, no. 2, pp. 185-191, Feb. 2017.
- [7] W. Shin, M. Vaezi, B. Lee, D. J. Love, J. Lee and H. V. Poor, "Coordinated beamforming for multicell MIMO-NOMA," *IEEE Commun. Lett.*, vol. 21, no. 1, pp. 84-87, Jan. 2017.
- [8] M. S. Ali, E. Hossain, A. Al-Dweik, and D. I. Kim, "Downlink power allocation for CoMP-NOMA in multi-cell networks", *IEEE Trans. Commun.*, vol. 66, no. 9, pp. 3982-3998, Sep. 2018.
- [9] Y. Fu, M. Zhang, L. Salaün, C. W. Sung and C. S. Chen, "Zero-forcing oriented power minimization for multi-cell MISO-NOMA systems: A joint user grouping, beamforming, and power control perspective," *IEEE J. Sel. Areas Commun.*, vol. 38, no. 8, pp. 1925-1940, Aug. 2020.

- [10] H. Zhang, H. Zhang, W. Liu, K. Long, J. Dong and V. C. M. Leung, "Energy efficient user clustering, hybrid precoding and power optimization in Terahertz MIMO-NOMA systems," *IEEE J. Sel. Areas Commun.*, vol. 38, no. 9, pp. 2074-2085, Sept. 2020.
- [11] Z. Wang, Z. Lin, T. Lv and W. Ni, "Energy-efficient resource allocation in massive MIMO-NOMA networks with wireless power transfer: A distributed ADMM approach," *IEEE Internet Things J.*, vol. 8, no. 18, pp. 14232-14247, 15 Sept. 2021.
- [12] Y. Shen, Y. Shi, J. Zhang and K. B. Letaief, "Graph neural networks for scalable radio resource management: Architecture design and theoretical analysis," *IEEE J. Sel. Areas Commun.*, vol. 39, no. 1, pp. 101-115, Jan. 2021.
- [13] A. Chowdhury, G. Verma, C. Rao, A. Swami and S. Segarra, "Unfolding WMMSE using graph neural networks for efficient power allocation," *IEEE Trans. Wireless Commun.*, vol. 20, no. 9, pp. 6004-6017, Sept. 2021.
- [14] X. Xu, Q. Chen, X. Mu, Y. Liu and H. Jiang, "Graph-embedded multi-Agent learning for smart reconfigurable THz MIMO-NOMA networks," *IEEE J. Sel. Areas Commun.*, vol. 40, no. 1, pp. 259-275, Jan. 2022.
- [15] J. Guo and C. Yang, "Learning power allocation for multi-cell-multi-user systems with heterogeneous graph neural networks," *IEEE Trans. Wireless Commun.*, vol. 21, no. 2, pp. 884-897, Feb. 2022.
- [16] T. Elsken, J. H. Metzen, and F. Hutter, "Neural architecture search: A survey," *J. Mach. Learn. Res.*, vol. 20, no. 55, pp. 1-21, 2019.
- [17] L. Ruiz, F. Gama and A. Ribeiro, "Graph neural networks: Architectures, stability, and transferability," *Proc. IEEE*, vol. 109, no. 5, pp. 660-682, May 2021.
- [18] S. Boyd, N. Parikh, E. Chu, B. Peleato and J. Eckstein, "Distributed optimization and statistical learning via the alternating direction method of multipliers," *Found. Trends Mach. Learn.*, vol. 3, no. 1, pp. 1-122, Jan. 2011.
- [19] M. F. Hanif, Z. Ding, T. Ratnarajah, and G. K. Karagiannidis, "A minorization-maximization method for optimizing sum rate in the downlink of non-orthogonal multiple access systems," *IEEE Trans. Signal Process.*, vol. 64, no. 1, pp. 76-88, Jan. 2016.
- [20] F. Hutter, L. Kotthoff, and J. Vanschoren, "Automated machine learning: methods, systems, challenges." Cham, Switzerland: Springer, 2019.
- [21] H. Liu, K. Simonyan, and Y. Yang, "DARTS: Differentiable architecture search," 2018, *arXiv:1806.09055*. [Online]. Available: <http://arxiv.org/abs/1806.09055>
- [22] M. Zhang, S. W. Su, S. Pan, X. Chang, E. M. Abbasnejad, R. Haffari, "iDARTS: Differentiable architecture search with stochastic implicit gradients," in *Proc. Int. Conf. Mach. Learn.*, Jul. 2021, pp. 12557-12566.
- [23] J. Lorraine, P. Vicol, and D. Duvenaud, "Optimizing millions of hyperparameters by implicit differentiation," in *Proc. 23rd Int. Conf. Artif. Intell. Statist.*, 2020, pp. 1540-1552.
- [24] Y. Bengio, "Gradient-based optimization of hyperparameters," *Neural Computation*, vol. 12, no. 8, pp. 1889-1900, 2000.
- [25] L. Franceschi, P. Frasconi, S. Salzo, R. Grazzi, and M. Pontil, "Bilevel programming for hyperparameter optimization and meta-learning," in *Proc. Int. Conf. Mach. Learn.*, Jul. 2018, pp. 1563-1572.
- [26] A. Shaban, C. A. Cheng, N. Hatch, and B. Boots, "Truncated back-propagation for bilevel optimization," in *Proc. 22nd Int. Conf. Artif. Intell. Statist.*, 2019, pp. 1723-1732.
- [27] R. Grazzi, L. Franceschi, M. Pontil, and S. Salzo, "On the iteration complexity of hypergradient computation," in *Proc. Int. Conf. Mach. Learn.*, Jul. 2020, pp. 3748-3758.
- [28] G. Stewart, *Matrix Algorithms: Basic Decompositions*, vol. 1, 1st ed. Cambridge, U.K.: Cambridge Univ. Press, 1998.
- [29] L. Dai, B. Wang, M. Peng and S. Chen, "Hybrid precoding-based millimeter-wave massive MIMO-NOMA with simultaneous wireless information and power transfer," *IEEE J. Sel. Areas Commun.*, vol. 37, no. 1, pp. 131-141, Jan. 2019.
- [30] J. P. Kermoal, L. Schumacher, K. I. Pedersen, P. E. Mogensen and F. Frederiksen, "A stochastic MIMO radio channel model with experimental validation," *IEEE J. Sel. Areas Commun.*, vol. 20, no. 6, pp. 1211-1226, Aug. 2002.
- [31] S. Boyd and J. Duchi, *EE364b: Convex Optimization II*. Stanford, CA, USA: Stanford Univ., 2008.